Funded by the European Union

Project Title:

Eco-operated, Modular, highly efficient, and flexible multi-POWERtrain for long-haul heavy-duty vehicles

Acronym: EMPOWER

Grant Agreement No.: 101096028

Topic: **Modular multi-powertrain zero-emission systems for HDV (BEV and FCEV) for efficient and economic operation (2ZERO)**

Topic identifier: **HORIZON-CL5-2022-D5-01-08**

Type of action: **Innovation Action (IA)**

Deliverable No.	D5.2	
Deliverable Title	Vehicle connectivity, V2G communication and eco-routing	
Deliverable Date	2025-04	
Deliverable Type	Report	
Dissemination level	Public	
Written by	Daniele ZONETTI (IFPEN) Nicolas POLLET (IFPEN) Olivier LEMAIRE (IFPEN) Antonio SCIARRETTA (IFPEN) Izaskun AIZPURUA (CID) Jon GOIBURU (CID) Jokin BATALLA (CID)	2025-03-15 to 2025-04-30
Checked by	Antonella ACCARDO(POLITO) Alessandro LICCARDO (LT) Claudio MEZZA (IVECO) Thomas BÄUML (AIT)	2025-05-02 to 2025-05-16
Approved by	Claudio MEZZA (IVECO)	2025-05-14

This project has received funding from the European Union's HORIZON EUROPE research and innovation programme under grant agreement No. 101096028. The content of this publication is the sole responsibility of the Consortium partners listed herein and does not necessarily represent the view of the European Commission or its services.

Status	Version 1.1 Version 1.2 Version 1.3 Version 1.4 Version 1.5 Version 1.6 Version 1.7 Version 1.8 Version 1.9	2025-03-20 2025-03-27 2025-04-22 2025-04-30 2025-05-06 2025-05-07 2025-05-07 2025-05-15 2025-05-16

This project has received funding from the European Union's HORIZON EUROPE research and innovation programme under grant agreement No. 101096028. The content of this publication is the sole responsibility of the Consortium partners listed herein and does not necessarily represent the view of the European Commission or its services.

Publishable Executive Summary

This deliverable reports the work realized within Task 5.2 ("Vehicle connectivity concepts and V2G communication") and Task 5.3 ("Eco-routing and fleet management tools") of the WP5 ("Innovative HVI, V2G communication, fleet management, and infrastructure"), and is subdivided in two parts.

The first part focuses on the charging process, both for a single vehicle and a vehicle fleet. Promising results in terms of energy efficiency, system performance, and practicality for real-time implementation were achieved. In the Single Vehicle Charging (SVC) the charging process efficiency is increased by current modulation that does not substantially affect charging time, while reducing peak power, which contributes to mitigating battery degradation. This charging method is then applied in the Smart Fleet Charging (SFC) where charging scheduling of 120 electric HDVs is defined. The power peak reduction obtained by applying efficient charging instead of fast charging is significant, being more than 50 %. While charging delay management becomes the main target of the SFC strategy. For that, different fleet charging criteria were compared and departure criteria turned out to be the more useful one, which gives priority to the vehicles that need to leave earlier the charging station. Additionally, this study provides insights into determining the optimal number of chargers for a given station, in order to balance installation costs and delay time. Moreover, the savings to be obtained by including renewable energy sources depends on the local demand and generation profiles, but it can be significant, reaching 81.85 % of savings in energy and power costs. Anyways, the potential for optimization in this field is significant, since multiple factors are involved.

The second part focuses on a cloud-connected system for the optimization of long-distance trips. First the system architecture is presented, both in terms of hardware and software. Then the strategies that will be implemented on the Iveco demonstrators are described with a certain detail. These comprise an eco-charging strategy for the optimization of the itinerary, the charging plan, and the cruising speed, as well as an eco-driving strategy for the optimization of the instantaneous speed profile. Results of simulations conducted along the project's demonstrator routes complete this part. The results obtained clearly demonstrate the effectiveness of the developed eco strategies in enhancing the performance, efficiency, and sustainability of electric heavy-duty vehicle operations. The eco-charging strategy consistently identified optimal itineraries that adapt to various user priorities—whether minimizing travel time, energy usage, or charging costs. Compared to a baseline strategy, optimized charging and routing plans lead to reductions in energy consumption of up to 12% (-77 kWh), savings in charging costs of over 20% (-34€), and a decrease in overall travel time of nearly 17% (-127 min), depending on the selected optimization criteria. Importantly, the developed ageing models also allows to measure battery degradation resulting from any of the optimal itinerary established by the eco-charging algorithm, therefore adding additional insight on the most convenient plan to be adopted for better preservation of the battery state of health. The eco-driving strategy, defined in cascade to the eco-charging strategy, further enhanced the system's energy efficiency by providing the vehicle's speed profile to be tracked by the driver to minimize energy consumption across different segments of the selected itinerary. This approach dynamically adjusted reference speeds in response to road geometry, legal limits, and slope variations, all while respecting the vehicle's dynamic constraints. The algorithm was proven particularly effective in road segments characterized by frequent acceleration and deceleration, such as in urban areas or areas subjected to a relevant variation of altitude, where it leverages regenerative braking and predictive speed control to reduce energy consumption. Applied to the route provided as output by the eco-charging algorithm, the eco-driving algorithm achieved a substantial energy saving of over 7%, equivalent to nearly 36 kWh.

Overall, the integration of smart charging and eco-strategies within a connected, integrated into a cloud-based architecture has proven to be a practical and impactful solution for next-generation electric freight mobility. The tools developed within this work package are thus ready to be deployed and validated on the IVECO demonstrators.

This project has received funding from the European Union's HORIZON EUROPE research and innovation programme under grant agreement No. 101096028. The content of this publication is the sole responsibility of the Consortium partners listed herein and does not necessarily represent the view of the European Commission or its services.

Table of Contents

This project has received funding from the European Union's HORIZON EUROPE research and innovation programme under grant agreement No. 101096028. The content of this publication is the sole responsibility of the Consortium partners listed herein and does not necessarily represent the view of the European Commission or its services.

List of Figures

This project has received funding from the European Union's HORIZON EUROPE research and innovation programme under grant agreement No. 101096028. The content of this publication is the sole responsibility of the Consortium partners listed herein and does not necessarily represent the view of the European Commission or its services.

List of Tables

This project has received funding from the European Union's HORIZON EUROPE research and innovation programme under grant agreement No. 101096028. The content of this publication is the sole responsibility of the Consortium partners listed herein and does not necessarily represent the view of the European Commission or its services.

Abbreviations and Nomenclature

Table 1: List of Abbreviations and Nomenclature

Symbol or Shortname	Description
APIs	Application Programming Interface
BEV	Battery Electric Vehicle
CAN	Controller Area Network
CasADI	Computer Algebra System with Automatic Differentiation
CCCV	Constant Current Constant Voltage
CSP	Constrained shortest path
DC	Direct Current
DOD	Depth of Discharge
EC	Eco-Charging
ECM	Equivalent Circuit Model
ED	Eco-Driving
e-HDV	electric Heavy-Duty Vehicles
e-LDV	electric Light-Duty Vehicles
EVs	Electric Vehicles
FEC	Full-Equivalent Cycle
GIS	Geographic Information System
GPS	Global Positioning System
gRPC	Remote Procedure Call (RPC) framework
HDV	Heavy-Duty Vehicles
HMI	Human Machine Interface
HVI	Heavy Vehicle Integration
ICE	Internal Combustion Engine
IPOPT	Interior Point OPTimizer
MILP	Mixed Integer Linear Programming
OCP	Optimal Control Problem
OCV	Open Circuit Voltage
PCM	Process Controle Module
SFC	Smart Fleet Charging
SOC	State of Charge
SOF	State of Function
SOH	State of Health
STD	Specific standard deviation
SVC	Single Vehicle Charging
V2G	Vehicle to Grid
VPPs	Virtual Power Plants
ZEV	Zero-Emission Vehicle

This project has received funding from the European Union's HORIZON EUROPE research and innovation programme under grant agreement No. 101096028. The content of this publication is the sole responsibility of the Consortium partners listed herein and does not necessarily represent the view of the European Commission or its services.

1 Introduction

This deliverable reports the work realized within Task 5.2 ("Vehicle connectivity concepts and V2G communication") and Task 5.3 ("Eco-routing and fleet management tools") of the WP5 ("Innovative HVI, V2G communication, fleet management, and infrastructure"). For the context and description of these subtasks, an extract from the project proposal is cited as the description is displayed below.

WP5
This WP aims at specifying and developing non-vehicle technologies that will be considered in the EMPOWER project.

Task 5.2
This task aims to explore Vehicle connectivity concepts and V2G communication enabling the opportunity to embrace EVs as distributed energy resources that are aggregated, optimised, and controlled by virtual power plants (VPPs) and distributed energy resource management systems.

- ***IFPEN** will set up the connectivity between the in-vehicle management strategies (Task 5.3) and its proprietary cloud.*

- ***CID** will analyse the suitability of any charging operation from the technical (C-rate) and economical (cost of the energy) point of view during diary charging and as virtual power plant. A charging strategy will be suggested to the driver or automatically applied prioritizing cost, operation, availability, or combinations of these parameters.*

Task 5.3
This task aims at developing connected solutions [eco strategies] for ZEV-specific, flexible (adapted to the characteristics of vehicles and infrastructure) managerial tools supporting the seamless integration of zero-tailpipe-emissions.

- ***IFPEN** will implement the eco-charging and eco-driving strategies and algorithms.*

- ***CID** will contribute to the charging and driving strategies led by IFPEN by embedding the medium/long term consequences in the battery.*

The remainder of the deliverable is organized in two main parts. Part 2, (led by CIDETEC) focuses on the charging process from the perspective of the physical operation of charging. This includes smart charging strategies and an ageing model for battery state-of-health estimation, which are key to understanding and optimizing how charging is performed. Part 3 (led by IFPEN), focuses on strategies to optimize the entire trip plan. This includes a combination of charging, driving, and routing choices to create an optimized charging plan that supports the vehicle's journey.

This project has received funding from the European Union's HORIZON EUROPE research and innovation programme under grant agreement No. 101096028. The content of this publication is the sole responsibility of the Consortium partners listed herein and does not necessarily represent the view of the European Commission or its services.

2 Charging strategies and battery ageing models

2.1 Task 5.2.

2.1.1 Vehicle charging and scheduling on a station

As the demand for e-HDV grows, efficient charging infrastructure and optimized scheduling play a critical role in ensuring operational efficiency, cost-effectiveness, and grid stability. Unlike passenger EVs, e-HDV require high-power charging, which increases energy demand and operational complexity.

Efficient charging strategies improve battery lifespan, reduce downtime, and optimize energy costs, while smart station scheduling prevents grid overload, minimizes wait times, and enhances fleet productivity. By integrating advanced algorithms, renewable energy sources, and real-time data, optimized charging solutions ensure that electric fleets operate seamlessly, supporting the transition to sustainable transportation.

In the context of T5.2, CID has been working on the development of an efficient vehicle charging methodology, called SVC, which is integrated into higher level SFC strategy for a charging station. Both are considered to be part of a route planner, as can be seen in the Figure 1.

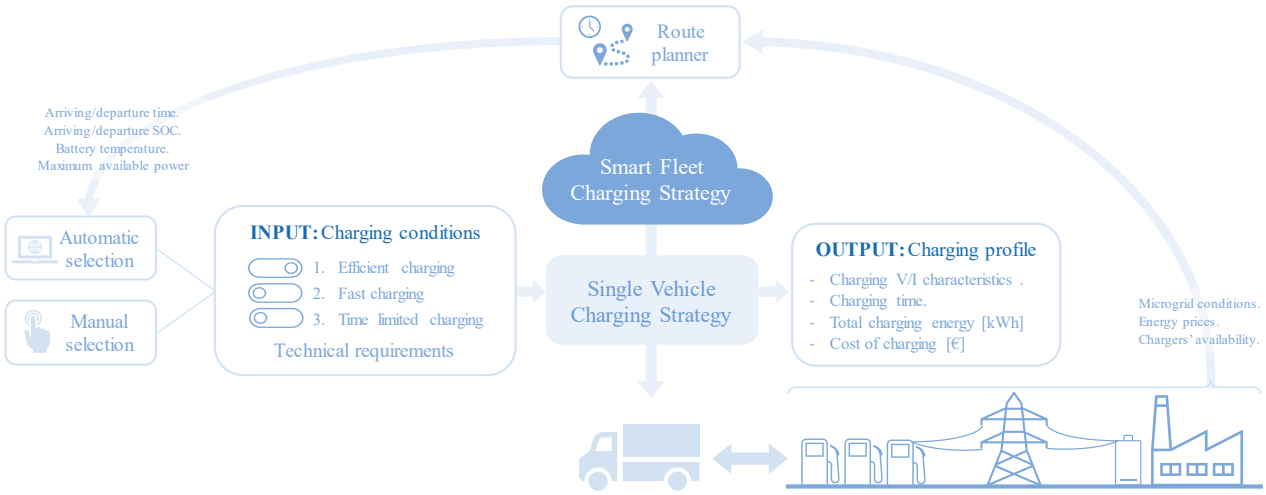

Figure 1: Vehicle level efficient charging and fleet level smart charging strategy.

The SFC is contextualized on a Truck operator's charging station. It schedules all the individual charging processes, considering all vehicles arrival and departure expectations, trying to optimize power exploitation, reduce peak power demand and total cost. It considers vehicle and charging station conditions such as priority, available charging points, individual charging SOC and time intervals, station power capacity or energy prices.

2.1.2 Single Vehicle Charging

The trend in HDV charging is to reduce charging time due to the high-capacity storage systems involved. However, prioritizing speed is not always the most efficient approach, as it can lead to higher energy losses and accelerated battery degradation.

To develop an optimized charging strategy for HDVs, existing charging methods have been analysed. Efficiency can be understood in different ways, such as Coulombic efficiency (the ratio of charged vs. discharged energy) or power conversion efficiency (minimizing losses in power electronics). In this case, the focus is on battery behavior during charging.

The standard charging method is constant current-constant voltage (CCCV), but several alternative strategies exist, as Figure 2 shows.

This project has received funding from the European Union's HORIZON EUROPE research and innovation programme under grant agreement No. 101096028. The content of this publication is the sole responsibility of the Consortium partners listed herein and does not necessarily represent the view of the European Commission or its services.

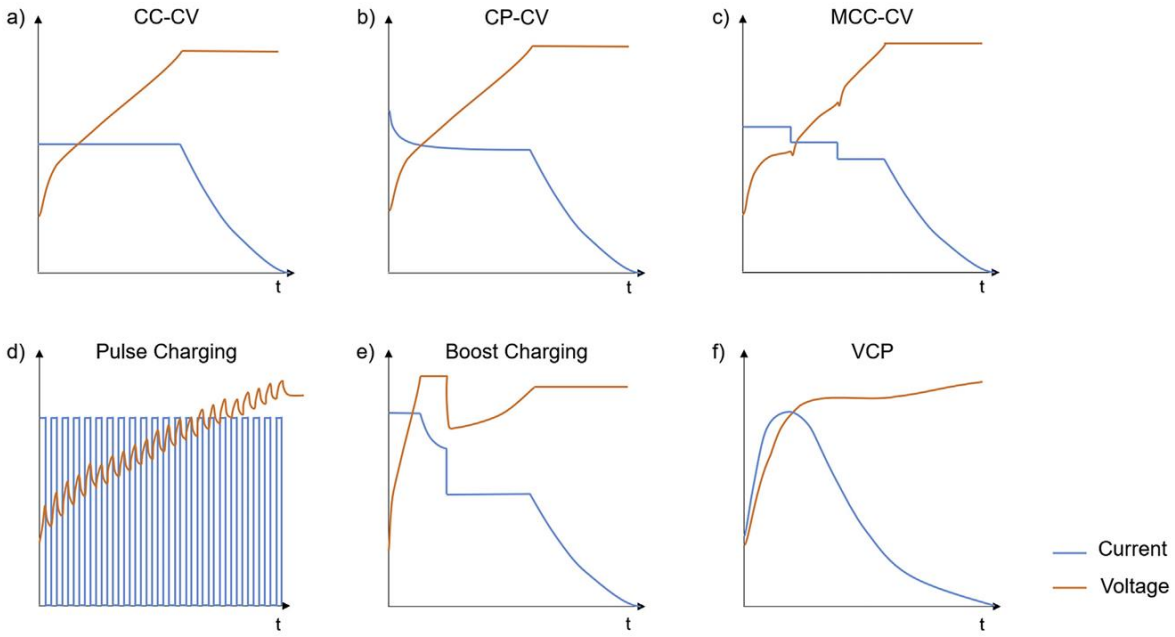

Figure 2: Existing charging techniques. [1]

These charging techniques are primarily used for fast charging. However, for greater efficiency, current modulation emerges as a promising alternative, as demonstrated in the work of Ahn and Lee [2], where the current profile is dynamically adjusted based on resistive behavior to minimize power losses. Their study indicates that this approach can reduce losses by up to 40% at a 1C charge rate, maintaining the same charging time. This improvement could increase charging efficiency from 83.6% to 89.5% without extending the charge duration.

In contrast, the study by Chen et al. [3] finds that the maximum reduction in losses occurs at a higher C-rate (3C), reaching 4.81%. These differences suggest that resistive behavior varies depending on battery technology, influencing the effectiveness of the methodology. They also consider charger/converter power losses when estimating overall system efficiency.

Nevertheless, even a small gain in efficiency can be significant for high-capacity systems, such as those used in electric HDVs, and even more so at a fleet level. Additionally, these studies do not account for the effects of current or temperature on internal resistance variations, which could help in optimizing efficiency further.

Therefore, instead of relying on the traditional CCCV charging method, an adaptive-current charging strategy is implemented in EMPOWER to assess its suitability and potential for improving efficiency. The proposed approach dynamically adjusts the charging current based on internal resistance, considering not only the SOC, but also previous C-rate and temperature, aiming to minimize energy losses.

Proposed methodology

The SVC defines the individual charging profile, considering charging necessities and charging mode selection. Three different charging modes are defined:

1. **Efficient charging:** Instead of classical CCCV charging an adaptive-current charging strategy is implemented. It consists of finding the optimal current depending on internal resistance, SOC and temperature to reduce energy losses.
2. **Fast charging:** High power-short time charging. As fast as possible without exceeding cell safety limits (State of Function, SOF), i.e. maximum C-rate depending on SOC and temperature.
3. **Time limited charging (≈ efficient):** In this case the charging follows the methodology of the efficient charging but charging time is fixed.

This project has received funding from the European Union's HORIZON EUROPE research and innovation programme under grant agreement No. 101096028. The content of this publication is the sole responsibility of the Consortium partners listed herein and does not necessarily represent the view of the European Commission or its services.

The charging profile is defined by an optimization problem which is adjusted to the selected charging strategy.

Input parameters

To conduct the optimization, it is essential to employ an ECM of the battery. IVECO's battery parameters were shared for this purpose.

From this data, internal resistance is mainly used for calculating power loss. However, power losses from other parts of the system, such as welding, busbars, and chargers, have not been considered. Additionally, the OCV charging curve is used to estimate cell voltage alongside the resistive voltage drop, but the dynamic voltage response due to capacitive behavior is not included, as the charging current is controlled, and significant variations are not expected over short time intervals. Moreover, thermal parameters were also considered, applying generic values for estimating the heat generation, heat transfer and cell temperature variation.

- 2nd order electrical parameters, from which only internal resistances are considered and not capacitors, SOC, current and temperature dependent.
- OCV is considered, which is SOC and temperature dependent.
- Generic thermal parameters: specific heat, and cell to ambient heat transfer equivalent resistance, considering convective cooling.

Apart from the modelling parameters, also operating limits are considered, which are the SOF based on operation conditions and the charger power limit, which is the technically maximum, or the available maximum due to external conditions.

- The SOF defines the maximum C-Rate depending on operation conditions: SOC and temperature.
- Maximum charger power available is considered, in this case, limited by the charger.

Electrical and thermal behaviour representation

For the definition of a charging profile by optimization, it has been necessary to define a reference variable, from which other charging variables can be estimated. For easier problem solving, SOC has been defined as the reference variable, since most of the electrical parameters are SOC dependent.

$$SOC^n = SOC_{init} + n \cdot \frac{SOC_{end} - SOC_{init}}{N} \quad (1)$$

where SoC^n is the SoC value for each interval, n is the interval number indicator, SOC_{init} is the minimum SoC considered for the charging interval, SOC_{end} is the maximum SoC limit, and N is the total number of intervals, defined to be 100. For example, if we fix SOC_{init} = 10% and SOC_{end} = 90%, the expression would be: SOC^n = 10% + n · 0.8%, being n ϵ {0, 1, 2, …, N}.

Once that reference SOC is defined, charging current and time per interval can be determined based on the reference SOC and Coulomb Counting expression.

$$SOC^n = SOC^{n-1} + {I_{ch}}^n \cdot \eta_{ch} \cdot \frac{{t_{interval}}^n}{3600 \cdot C_{cell}}, \quad (2)$$

where ${I_{ch}}^n$ is the charging current per interval in [A], η_{ch} is the efficiency of the charging process, ${t_{interval}}^n$ is the time duration per interval in [s], and C_{cell} is the cell capacity in [Ah].

Temperature is also a factor affecting various battery parameters, including performance, and efficiency. The cell temperature depends on its heat capacity, internal heat generation, and heat transfer to the ambient. The heat generation within the cell is mainly due to resistive losses (Joule heating) and reversible heat generation due to entropy change in the cell's electrochemical reactions. While heat dissipation from the cell to the ambient is modeled using an equivalent thermal resistance, based on Fourier's law of thermal conduction, assuming steady-state heat transfer. Therefore, the cell temperature behavior is modelled by the heat balance equation.

This project has received funding from the European Union's HORIZON EUROPE research and innovation programme under grant agreement No. 101096028. The content of this publication is the sole responsibility of the Consortium partners listed herein and does not necessarily represent the view of the European Commission or its services.

$$T_{cell}{}^{n} = T_{cell}{}^{n-1} + \left(Q_{gen}{}^{n} - Q_{cell\rightarrow amb}{}^{n}\right) \cdot \frac{t_{interval}{}^{n}}{Cp_{cell}}, \quad (3)$$

where $T_{cell}{}^{n}$ is the cell temperature per interval in [K], $Q_{gen}{}^{n}$ is the heat generation of the cell per interval in [W], $Q_{cell\rightarrow amb}{}^{n}$ is the heat transfer from cell to ambient per interval in [W], and Cp_{cell} is the cell specific heat capacity in [J/K].

After that, it is necessary to obtain SOC and temperature dependency expressions for multiple variables, because no interpolation or boolean conditions are permitted when formulating optimization problems. From one side, the internal resistance and OCV as representative of the electrical behavior of the cell. From the other side, the SOF ensuring safety operation limits.

- **Internal resistance:** one plane per SOC interval, with quadratic dependence on both current and temperature.
- **OCV:** temperature dependent 2nd order polynomial expression per SOC interval.
- **SOF:** 1) a non-linear ramp that varies according to temperature and 2) a maximum SOF value for each SOC.

Additional variables, such as charging voltage and power, are determined using standard electrical equations. The charging voltage is calculated by adding the resistive voltage drop to the OCV, and the charging power accounts for both the useful power delivered to the battery and the power losses due to internal resistance.

Objective function

A final step, before going into the optimization, is defining the objective function and the priorities. In order to develop a single methodology for all charging modes, both charging time and power loss are considered in the objective function, which can be seen on the next expression.

$$\boldsymbol{min}(\boldsymbol{A} \cdot Charging\ Loss + \boldsymbol{B} \cdot Charging\ Time) \quad (4)$$

$$\boldsymbol{Charging\ Loss}: \ E_{loss} = \sum_{n=1}^{N} R_{int}{}^{n} \cdot (I_{ch}{}^{n})^2 \cdot \frac{t_{interval}{}^{n}}{3600} \quad (5)$$

$$\boldsymbol{Charging\ Time}: \ T_{charge} = \sum_{n=1}^{N} \frac{t_{interval}{}^{n}}{3600} \quad (6)$$

where $Charging\ Loss$ is in [W], and $Charging\ Time$ in [s], E_{loss} is the cell total cell energy loss during charging due to resistive behaviour in [Wh], and T_{charge} is the total charging time in [h].

A and B weight factors are used to balance the weight of each term in the objective function. For that, A and B are divided by the corresponding maximum charging loss or minimum charging time, respectively, to normalize both variables.

In case of the fast charging, only charging time needs to be minimized so A=0 and B=100 is defined in this mode. As a result, the optimization problem tends to reduce the time intervals by increasing the current while respecting the charging boundaries, such as voltage, power and SOF.

However, for the time-limited charging, only charging power losses are minimized, by defining A=100 and B=0, and additionally the maximum charging time is limited to the selected value. Therefore, apart from modulating the charging current depending on internal resistance, the optimization problem tends to extend as much as possible the charging time (limited to the desired value) to reduce the power losses.

On the contrary, in the efficient charging mode, the charging time is not defined. Consequently, this factor needs to be also optimized, otherwise, the tendency to reduce charging losses results in extending to the infinite charging time. For that, a sensitivity analysis is carried out to define the values of A and B. There is no need to find the optimal combination of A and B values, but the relation between them. Figure 3 shows the effect of varying B, with a fixed value of A=200. From there, B=120 was selected, considering a 30 % of time

This project has received funding from the European Union's HORIZON EUROPE research and innovation programme under grant agreement No. 101096028. The content of this publication is the sole responsibility of the Consortium partners listed herein and does not necessarily represent the view of the European Commission or its services.

extension as the maximum admissible for the charging to be considered efficient. The reference is the fast charging being a 1.77 h charge with 9.1 kWh power loss at system level.

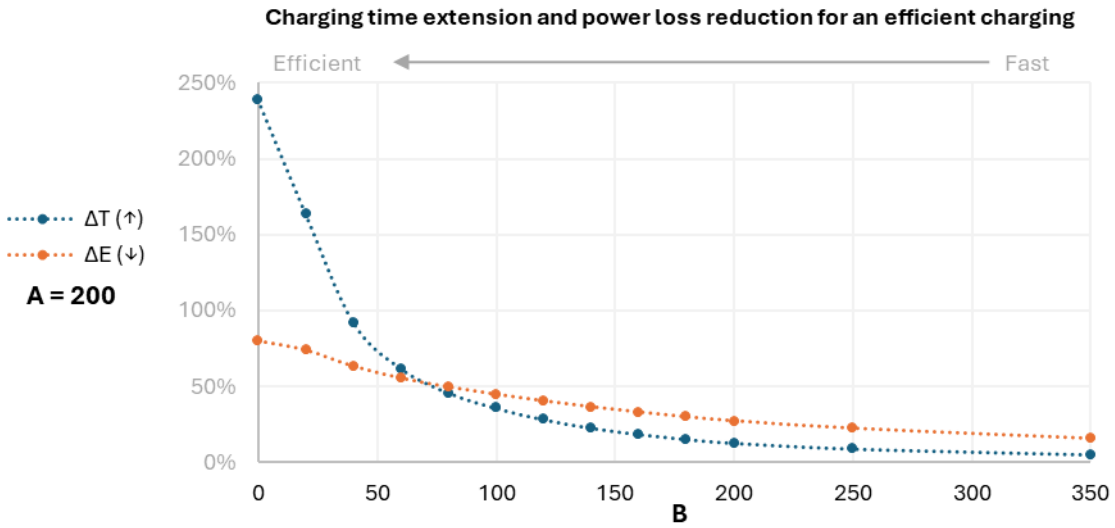

Figure 3: Sensitivity analysis of optimization power loss (A) and charging time (B) weights. Charging time extension and cell level power loss reduction with respect to the fast charging.

Optimization problem formulation

After defining all the necessary parameters and variables, the optimization problem is formulated as stated in Table 2. This optimization problem can be applied for all charging modes. It has been developed in the Matlab environment, solved using the *fmincon* solver which finds the minimum of a constrained non-linear multivariable function.

Table 2: SVC optimization problem.

OPTIMIZATION PROBLEM	
Objective function	**min**(**A** · Charging Loss + **B** · Charging Time) Efficient → A = 200 & B = 120 Fast → A = 0 & B = 100 Time-limited → A = 100 & B = 0
Variables	• Charging current • Internal resistance • Time intervals • OCV • Charging temperature
Constraints	• SOF • SOC variation • Cell temperature variation • SOC limits • Voltage limits • Charger power limit • Maximum charging time
Parameters	• SOC profile (range and intervals) • Internal resistance behavior parameters • OCV behavior parameters • Thermal behavior parameters • SOF variation parameters

Single Vehicle Charging results

In the next section the results obtained with the SVC are presented.

This project has received funding from the European Union's HORIZON EUROPE research and innovation programme under grant agreement No. 101096028. The content of this publication is the sole responsibility of the Consortium partners listed herein and does not necessarily represent the view of the European Commission or its services.

In Figure 4, cell level current profiles for different charging modes are shown. It can be easily noticed that fast charging (blue line) finishes first and it also has the highest current and power values limited by the SOF but also by the maximum power available. This means, that, even if the system could be charged faster, the charger cannot supply the necessary power level.

With the efficient charging mode, efficiency is improved with respect to the fast charging due to charging time extension (red line with respect to the blue one in Figure 4 (b)) and current modulation (red line with respect to the yellow one in Figure 4 (c)). Compared to fast charging, in efficient charging the charging time is extended by 28.18 %, resulting in a 2.27 h charge. Consequently, power losses are reduced by 40.35 % to 5.42 kWh. Additionally, peak power is reduced by 60.15 %, from 687.03 kW to 273.81 kW, which helps on reducing degradation and maximum temperature during charging.

The purple line in Figure 4 corresponds to the time-limited charging, for which charging time can be fixed instead of optimized. This charging mode is equivalent to the efficient-charging considering that the modulation strategy is also applied, but it is a more friendly to use set-up since the final user could define this charging time. Although when thinking about a whole station scheduling the whole system optimization can be more interesting, which is not possible if the charging time is fixed.

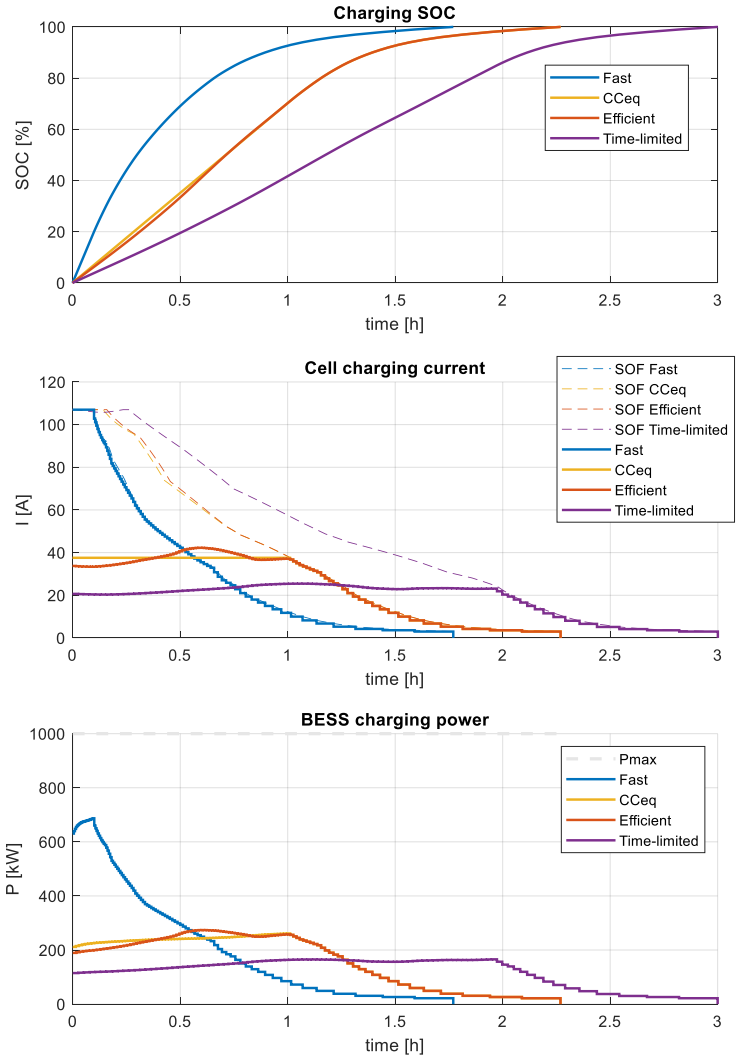

Figure 4: Results of SVC modes. (a) SOC charging profile, (b) current profile at cell level, and (c) power profile at system level.

This project has received funding from the European Union's HORIZON EUROPE research and innovation programme under grant agreement No. 101096028. The content of this publication is the sole responsibility of the Consortium partners listed herein and does not necessarily represent the view of the European Commission or its services.

In Figure 5, the efficient charging mode can be understood more deeply, where current modulation and its effect can be observed. There is a compensation between internal resistance increment and charging current reduction, and vice versa, for power loss reduction (referred as electric power loss). Voltage and temperature evolution can be also observed, which remains inside safety limits.

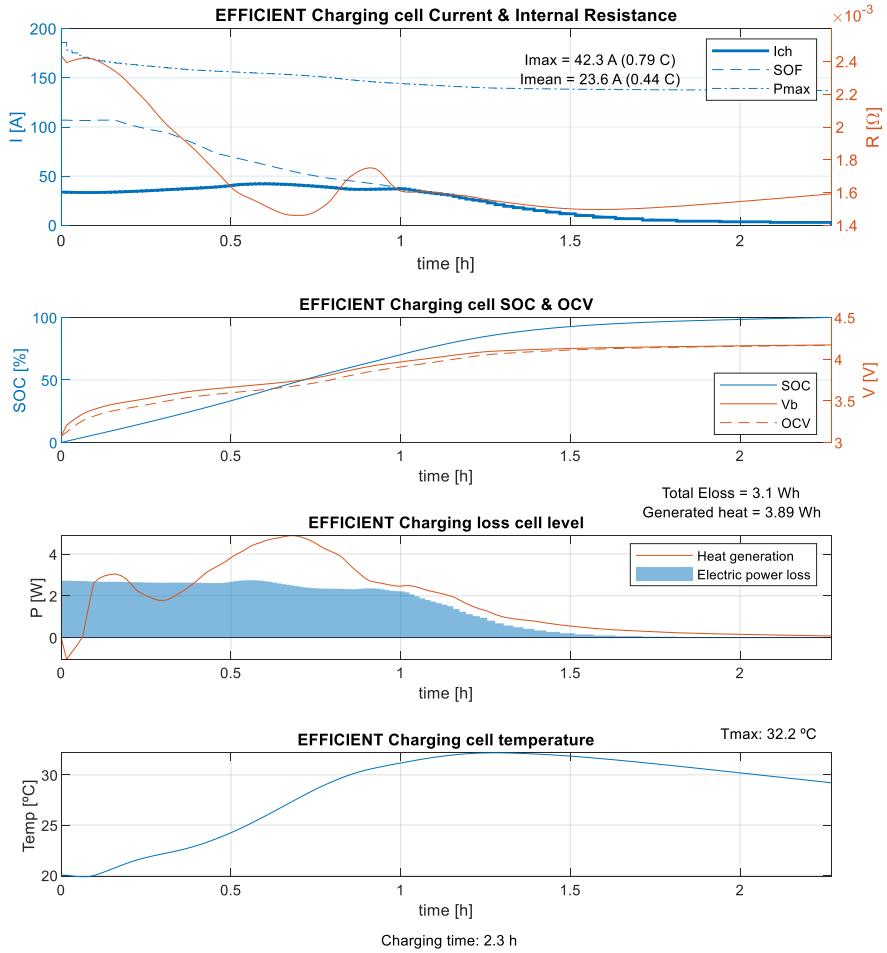

Figure 5: Efficient charging current modulation and charging evolution at cell level.

2.1.3 Smart Fleet Charging

The developed SVC strategy is integrated into the SFC. The objective is to define the optimal charging scheduling of the vehicles in a station for cost reductions, coordinating the charging demand with the station consumption and generation. Both the charging station and the fleet belong to a logistics and transportation company seeking to optimize the management of charging points and energy usage, improving operational efficiency.

Several studies have focused on optimizing energy management and charging strategies for electric vehicle (EV) fleets, but there has been limited work addressing the specific scheduling of vehicle charging based on demand, generation, and prioritization. For instance, Dang et al. [4] explore the concept of EV fleets as virtual battery resources for community microgrid energy storage, providing a foundation for integrating EVs into local grid management. Golder and Williamson [5] review energy management systems (EMS) for EV charging stations, focusing on the overall management of fleet energy rather than detailed scheduling of charging times.

This project has received funding from the European Union's HORIZON EUROPE research and innovation programme under grant agreement No. 101096028. The content of this publication is the sole responsibility of the Consortium partners listed herein and does not necessarily represent the view of the European Commission or its services.

Awad et al. [6] investigate resource allocation and charging pricing within smart electric vehicle parking lots, aiming to maximize overall fleet efficiency. Similarly, Wang et al. [7] focus on the simulation and management strategies of charging stations, especially in the context of DC microgrids, which could be applied to fleet charging scenarios. Xu et al. [8] propose a scenario where EV batteries could serve as a storage solution for the grid, highlighting the broader potential of EV fleets to support grid demand.

Additionally, some studies are already analyzing how to coordinate the charging of EV fleets in parking lots, such as [9] in which a three-stage energy management is proposed: 1) day-ahead planning, 2) real-time power management, and 3) priority-based EV charging. But the optimization is developed at parking level, considering aggregated charging demand. In case of [10] charging profile of single vehicle is considered, but classical CCCV charging method is applied, and linearized for the optimization of operation. The objective is to maximize total profit and reduce battery degradation, by defining when it is interesting to charge, and choosing between fast or normal charging.

Although various studies have explored EV fleet energy management, they tend to emphasize dynamic storage capacities, energy resource allocation, and they often focus on high-level optimization frameworks, considering aggregated demand management, rather than directly addressing practical scheduling strategies. However, when scheduling and individual charging profiles are analyzed, they rely on complex optimization methods, or optimize aggregated charging demand, without explicitly considering efficiency or thermal behavior. These approaches, though valuable, do not offer a simple and adaptable scheduling strategy that balances cost reduction, operational efficiency, and station energy coordination. This gap motivates the development of the proposed SFC strategy, which introduces a priority-based approach to scheduling, ensuring a more practical integration of fleet charging with station consumption and local generation.

Initial comparison analysis

Before defining any specific SFC strategy, a comparison of different criteria is performed to evaluate the effect of them. To begin with, the SFC only seeks to schedule the charging of the vehicles, without considering any local demand or generation.

The scheduling methodology is based on defining charging priority and order, based on a previously defined vehicle arrival time/SoC, target SoC, and planned departure time. Consequently, a charging time interval for each vehicle is assigned. The specific charging profile is defined by the efficient SVC considering the charging limits or conditions (already mentioned predefined parameters of arrival and departure). The effect of modifying the scheduling criteria is reflected in the charging priority and therefore the charging order or time interval.

At the end, the scheduling consists of estimating the station queue and selecting the vehicle with higher priority (depending on criteria) when a charger is available. This way a charging slot for each vehicle is defined.

Scheduling methodology

For that, first, efficient SVC is applied to every vehicle since vehicle arrival time and SOC, as well as target SOC and expected departure time are known in advance. These parameters are considered to be inputs coming from a higher-level route planner. This way, each vehicle's charging time can be estimated.

0. **Define charging profile (applying efficient charging mode)** → Considering arrival and target SOC, available maximum charging time (difference between planned departure and expected arrival time) as well as cell parameters and battery system configuration, efficient SVC is applied to define charging time and power profile of each vehicle.

This project has received funding from the European Union's HORIZON EUROPE research and innovation programme under grant agreement No. 101096028. The content of this publication is the sole responsibility of the Consortium partners listed herein and does not necessarily represent the view of the European Commission or its services.

These charging profiles are always considered independently of the criteria. Even if the criteria affect the charging scheduling, each vehicle's charging profile remains the same. Therefore, the next steps are followed for the comparison of the criteria:

1. **Define charging priority (depending on criteria):** Depending on the defined criteria, a priority level is defined for each vehicle. This is not directly translated as an actual order, but as a symbolic priority when defining the charging slot for each vehicle. This means that the vehicle with higher priority does not necessarily have to be the first to arrive or be charged, but it would have the priority respect to the rest of the vehicles when arriving to the station.
2. **Schedule charging time →** As mentioned, depending on the priority previously defined, the charging slot for each vehicle is assigned. The priority is evaluated between the vehicles in the queue instantly. When a charger becomes empty, the current queue is checked to find the vehicle with highest priority between them, and that would be the one to be next in charging, and the charging slot for that vehicle is assigned.
3. **Simulate fleet behaviour →** Finally, the scheduled charging of vehicles is simulated and both power and time adjusted to a more realistic situation. This way, final power values and aggregated cost is calculated.

The limitation for both scheduling and simulation is the number of chargers in the station. The peak power per charger should also be considered, but it is not expected to be reached because when charging profile is defined, with efficient charging mode, power limits are already considered and respected.

The cost estimation is divided into three components: energy, power and delay cost. In this case, as mentioned, they correspond only to the charging profiles of the station.

- **Energy cost →** It is the cost of the consumed energy depending on power profile, periods and tariff. It can be calculated for every vehicle or aggregated for the station. The energy per time interval is multiplied by the corresponding energy cost composed of access toll and production cost.
- **Power cost →** It corresponds to the cost of peak power per period, which applies to aggregated power, and therefore there is no power term cost referring to single EVs, but for all the station. There are three different power periods: low [0:00-8:00), medium [8:00-9:00) U [14:00-16:00) U [22:00-24:00), and peak [9:00-14:00) U [16:00-22:00). So, first, peak power is calculated and then the corresponding cost, which also depends on tari and period.
- **Delay cost →** It applies only to the vehicles that depart later than expected, which implies cost losses due to delay in arrival of goods or similar. Each vehicle depending on their route and carried products has a different delay cost associated. The delay time is estimated and the corresponding cost calculated.
- **Total cost →** It is the resulting cost, when adding all energy, power and delay costs. In case of EV total cost, only energy and delay costs would be considered.

Definition of scenarios

To compare the different criteria, it is important to contextualize the station setup. The defined charging station consists of 10 chargers, each with a maximum power capacity of 1 MW. It is expected that 120 electric HDVs arrive and are charged during a day (24 h), with predefined arrival time, arrival SOC, target SOC and maximum charge times. Each vehicle has different delay costs, which range from 10-250 €/h, based on references [11], [12], [13].

Additionally, to ensure that the conclusions drawn are useful and not limited to a specific scenario, vehicle parameters are varied to generate different scenarios simulating various charging needs.

This project has received funding from the European Union's HORIZON EUROPE research and innovation programme under grant agreement No. 101096028. The content of this publication is the sole responsibility of the Consortium partners listed herein and does not necessarily represent the view of the European Commission or its services.

Table 3 defines the input parameters and the permitted range, based on which the scenarios are generated randomly following a normal distribution with a mean value and a specific standard deviation (STD) to emulate a realistic scenario. Besides, Figure 6 shows an example of input data of a specific scenario which will be further analysed in the next sections.

Table 3: Input parameters' permitted range.

HDV number	Arrival time	Arrival SOC	Departure time	Target SOC	Delay cost
EVXXX	00:00-24:00 Mean: 11:00 STD = 6 h	10-60 % Mean: 30 % STD = 10 %	Stay time = 1.5-4 h Departure < 04:00 (+1)	50-95% Mean: 80% STD = 15% ΔSOC > 20%	10-250 €/h

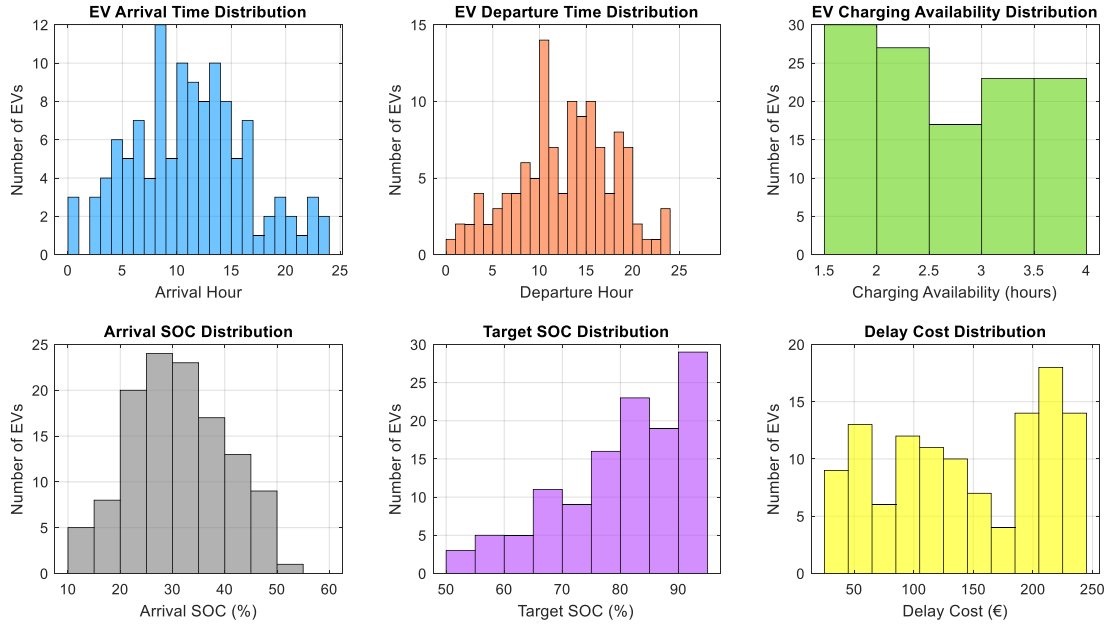

Figure 6: Example of predefined electric HDVs input data for the scheduling.

Comparison of results

The different criteria for the comparison of results are the following ones:

- **CRITERIA A = Arrival:** Vehicles starts charging as soon as they arrive, in arrival order.
- **CRITERIA D = Departure:** First vehicle departing (planned) is first in order.
- **CRITERIA C = Charging time:** The vehicle with shorter charging time (defined by the efficient charging) is first in order.
- **CRITERIA S = SOC range:** The vehicle with shorter charging SOC range (difference between target and arrival, defined externally) is first in order.
- **CRITERIA DC = Delay cost:** The vehicle with higher delay cost has the priority and is the first in order.
- **CRITERIA F = Flexibility:** The vehicle with lower flexibility has the priority and is the first in order.

The results obtained by comparing the different criteria in different scenarios (all with 120 vehicles) are summarized in Figure 7, where minimum, mean and maximum of the obtained results for each criterion are presented. From there, the more effective criteria can easily be identified, which is the departure time. Prioritizing the vehicles with earlier planned departure time in the queue makes the overall delay cost to be minimized. This is due to the reduced number of delayed vehicles, which remains below 10 and the corresponding total delay time, below 2h.

This project has received funding from the European Union's HORIZON EUROPE research and innovation programme under grant agreement No. 101096028. The content of this publication is the sole responsibility of the Consortium partners listed herein and does not necessarily represent the view of the European Commission or its services.

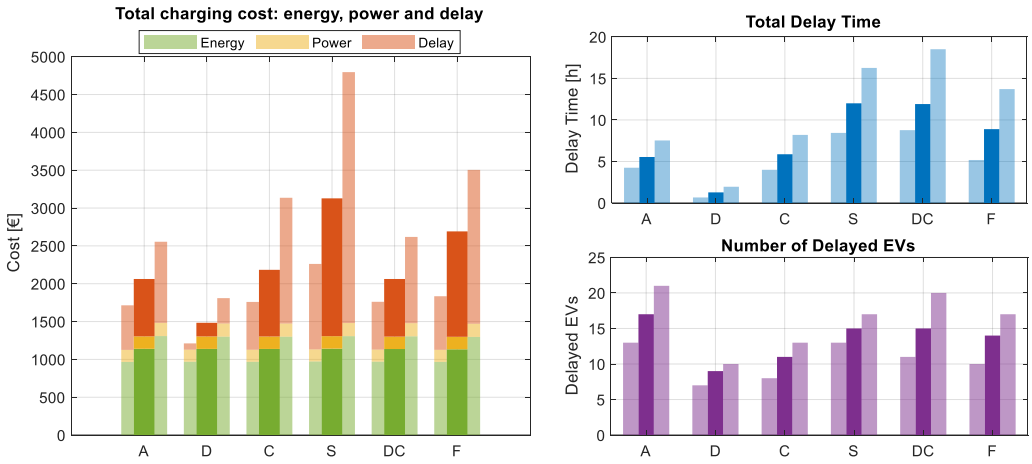

Figure 7: SFC criteria comparison results in different scenarios (min, mean and max for each criteria).

In depth analysis of results

Departure criteria scheduling example

One of the simulated scenarios, and the results obtained by applying the departure criteria (D), are presented below. The input about arrival/departure time and SOC are shown in Figure 6.

Figure 8 (c) shows the charging power evolution during the day, where aggregated charging demand is visualized and vehicle charging profiles are differentiated by colours. Moreover, simultaneous charges are presented (Figure 8 (b)) and queue length evolution (Figure 8 (a)). There is no significant queue until 8 a.m. approximately, and the maximum number of vehicles waiting is 10, which implies at most one vehicle per charging point. From 5 a.m. to 8 p.m. the number of simultaneous charges is near 10, which means that the charging demand is high and consequently the power demand also, but with high variation due to dynamics of charging profiles and connection and disconnections. This makes station management and vehicle scheduling necessary.

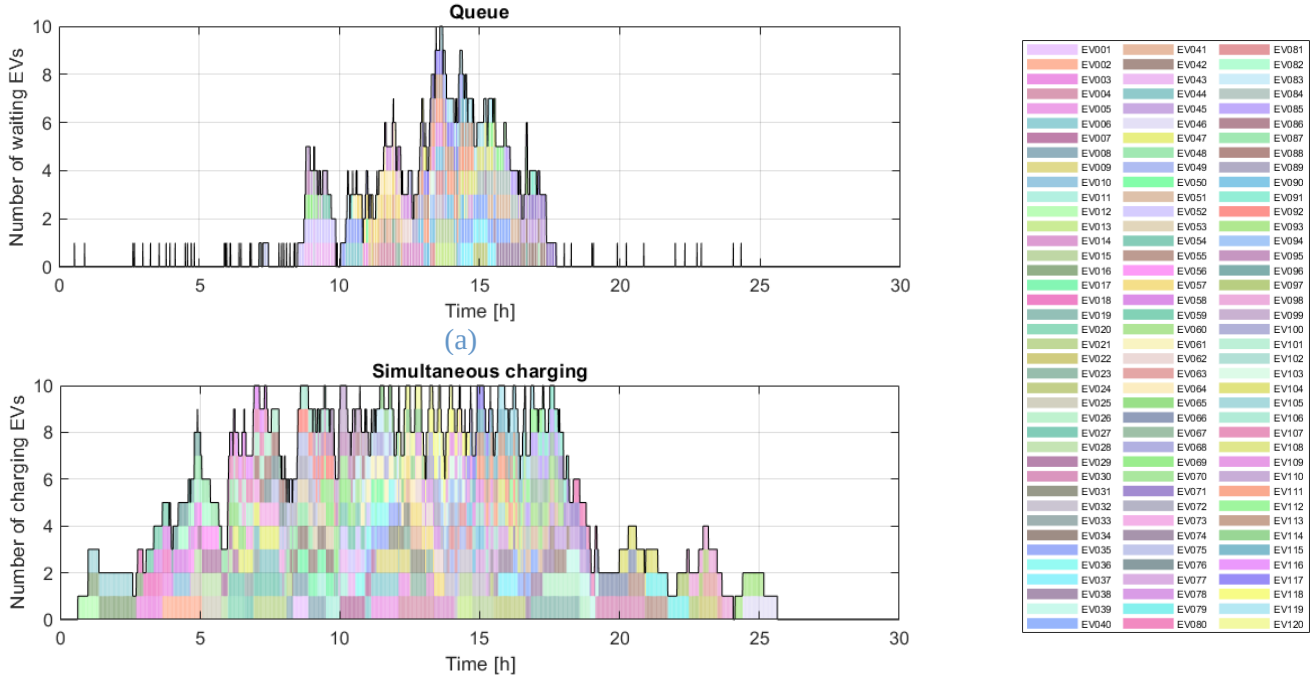

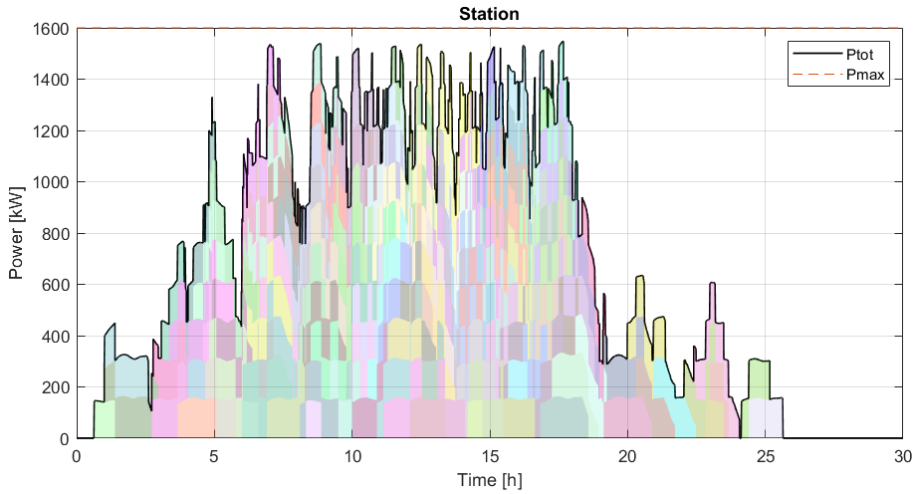

(c)

Figure 8: Station charging demand, with departure (D) criteria in the selected scenario. (a) Queue evolution, (b) simultaneous charges, and (b) aggregated power demand.

In Figure 9, the scheduling of the vehicles and chargers' usage can be observed. There we can see that from 9 a.m. to 5 p.m. chargers are continuously full which means that there is no room for advancing or delaying vehicles without modifying the defined charging time and profile. This also means that chargers are highly optimized. In these simulated scenarios, chargers 1 and 2 are more exploited, as they are the first to be demanded by default when a vehicle arrives, but in a more realistic situation the use of chargers should be more spread out.

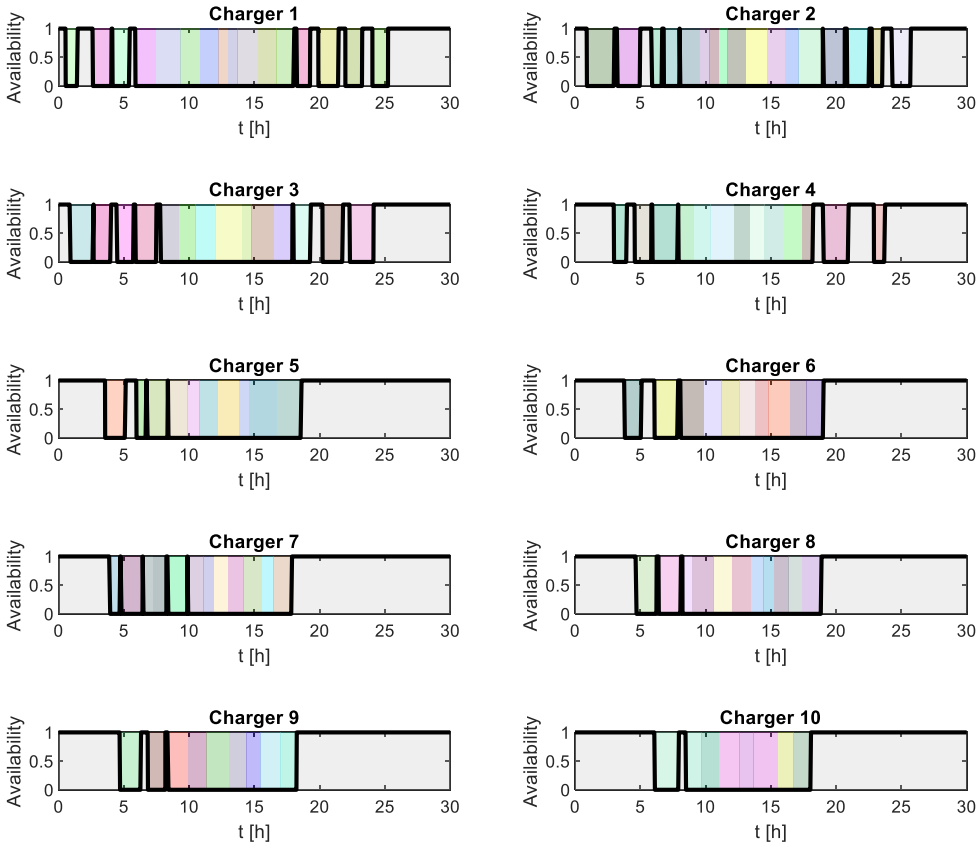

Figure 9: Chargers' availability and vehicles' scheduling, with departure (D) criteria in the selected scenario.

This project has received funding from the European Union's HORIZON EUROPE research and innovation programme under grant agreement No. 101096028. The content of this publication is the sole responsibility of the Consortium partners listed herein and does not necessarily represent the view of the European Commission or its services.

Figure 10, shows the charging, waiting and delay time, and flexibility distribution. There it can be seen that the charging time is around 1 h, and at most 2h. It can also be seen that flexibility is mostly above 30 %, meaning that charging time is limited, leaving a margin for waiting time due to high charging demand. Anyways, delays are mostly avoided. In all cases the delay is less than one hour, and if any, it is mostly less than 15 minutes (0.25 h). Additionally, the waiting time of most of the vehicles is also below 15 minutes.

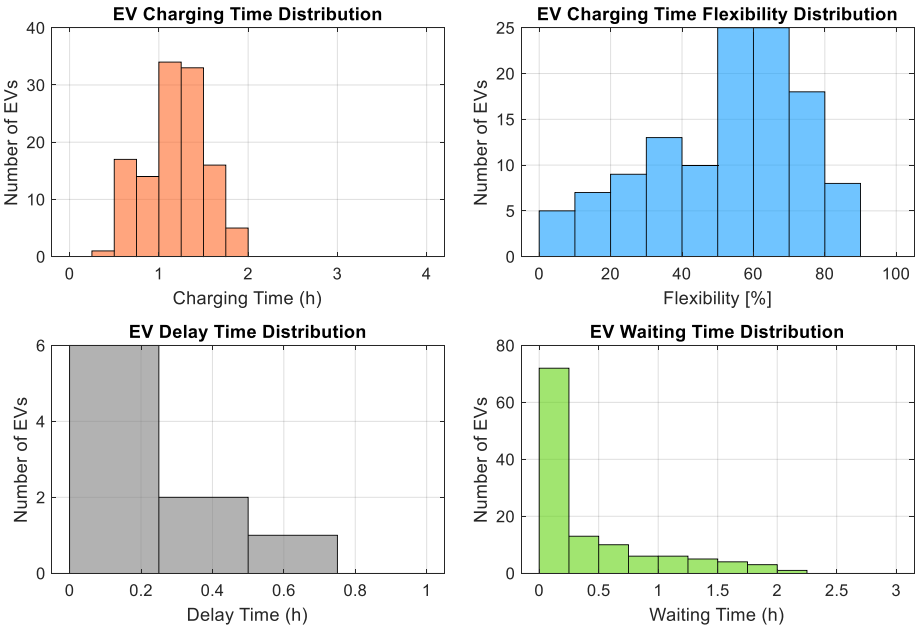

Figure 10: Distribution of charging, waiting and delay time of vehicles, and flexibility when applying departure criteria, in the selected scenario.

In Figure 11, delayed vehicles can be easily identified. There, time intervals are shown in percentage with regard of the available time, which is the difference between planned departure and arrival time, which is the interval where charging should be fulfilled. The yellow color indicates the waiting time, which is preferrable to be avoided, and the green one is the remaining time before departing. However, the red color indicated the delay time, which is the one to be avoided, and the corresponding number of chargers can also be observed.

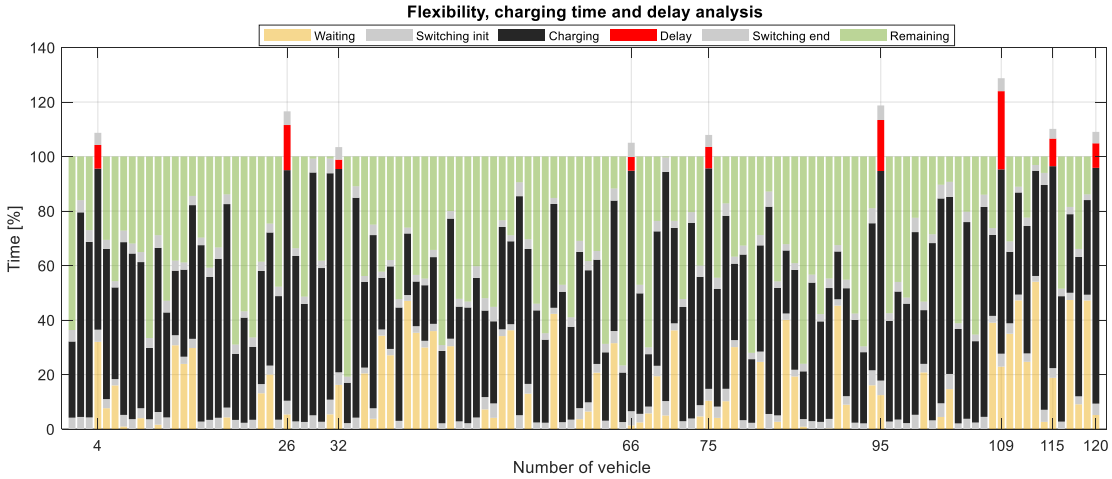

Figure 11: Percentage of waiting, charging, delay and remaining time of vehicles, when applying departure (D) criteria, in the selected scenario.

This project has received funding from the European Union's HORIZON EUROPE research and innovation programme under grant agreement No. 101096028. The content of this publication is the sole responsibility of the Consortium partners listed herein and does not necessarily represent the view of the European Commission or its services.

Although in Figure 11 it might appear that there is an excess of additional charging time (green colour), this time is necessary so that the next vehicle can be charged without generating cumulative delays.

Analysis the charging and waiting time of delayed vehicles, the main reason of delay can be identified. Most of the vehicles were delayed since the waiting time was higher than the flexible time. But, there is one vehicle (nº 26), that even defined charging time was higher than the available one. In some cases (vehicles nº 32 and 66), even if charging time and waiting time was lower than the available, which is desirable, but connection and disconnection time is also a factor to be considered, which at the end can cause the vehicle to be delayed.

Departure criteria scheduling improvement

To improve scheduling and avoid delays, vehicle charging times can be adjusted by either limiting or extending them based on each vehicle's expected departure time, and next vehicle charging time. For vehicles that are already delayed, fast charging can be applied to recover time. However, a more convenient approach involves setting the maximum charging duration considering the departure time, and apply time-limited charging mode, to avoid delay while still improving efficiency. In case of vehicles with flexible margins, extending the charging time can further enhance efficiency, either by starting earlier or prolonging the session when possible. These changes require only slight modifications to the current scheduling system.

As a reference, necessary adjustments were estimated to reduce costs by up to 12.14%, by avoiding delay cost. At the same time, energy cost variation should be considered, since charging profiles would be modified. Anyways, it should remain similar since most modifications would occur during low or medium energy price periods (estimated variation of ±4%).

Station charging point vs. vehicles analysis

To analyze the relationship between the number of vehicles and available charging points, a scenario with 150 electric HDVs and 10 chargers was simulated. The results showed a significant increase in queue length, waiting times, and delayed departures compared to the previous scenario, as shown in Table 4. The queue grew from a maximum of 10 to nearly 30 vehicles, with some waiting times exceeding 4 hours. Additionally, 86 vehicles experienced delays, some reaching up to 3 hours, while in the earlier scenario, delays remained under one hour.

With this analysis, it would be possible to define the necessary number of chargers or charging points. In this case, it is clear that 10 chargers for 150 vehicles are not sufficient. However, the solution is not simply to oversize the charging station. Instead, an optimal number of chargers should be defined based on operational needs. Moreover, SFC scheduling can help on maximizing chargers' usage optimizing infrastructure investment.

Table 4: Evaluation of electric HDVs number effect for the same number of charging points.

	150 electric HDVs	**120 electric HDVs**
Maximum queue length	**29**	**10**
Mean waiting time	1.54 h	25.77 min
Maximum waiting time per vehicle	**4.63 h**	**2.24 h**
Number of delayed vehicles	**86**	**9**
Maximum delay time per vehicle	**2.87 h**	**0.51 h**
Total delay time	77.01 h	1.96 h

This project has received funding from the European Union's HORIZON EUROPE research and innovation programme under grant agreement No. 101096028. The content of this publication is the sole responsibility of the Consortium partners listed herein and does not necessarily represent the view of the European Commission or its services.

Efficient vs. fast charging effect in station

Finally, it is interesting to check the improvements of efficient charging modes with respect to fast charging. As mentioned in previous sections, at first, reducing waiting time, and avoiding delay time should be the main objective of a fleet charging scheduling. However, in this study efficiency is also a factor to be improved, that is why fast charging becomes not desirable, due to higher energy losses and degradation impact.

In the Table 5, the comparison between fast and efficient SFC can be observed. There, expected results appears such as no delay, lower waiting time and shorter queue in the fast charging, and a higher energy efficiency, and lower vehicles' unused time in case of efficient charging. However, there is an additional factor which has also a significant difference, which is the peak power demand for charging. Even if mean power values are similar, peak power values are very different, being the peak power with fast charging (3.35 MW) more than double. This would be translated to a higher grid connection capacity need and degradation to both vehicles' storage and chargers. Therefore, this reinforces the idea that reducing power level by efficient charging mode is convenient, always working inside permissible range (arrival and departure time).

Table 5: Comparison between fast and efficient SFC.

	FAST charging	**EFFICIENT charging**
Mean charging time	0.65 h	1.18 h
Maximum charging time	1.13 h	1.99 h
Maximum queue length	**1**	**10**
Mean waiting time	5.07 min	25.77 min
Maximum waiting time per vehicle	**9.63 min**	**2.24 h**
Number of delayed vehicles	**0**	**9**
Maximum delay time per vehicle	0 h	0.51 h
Total delay time	0 h	1.96 h
Chargers idle time	**74 %**	**52.86 %**
Energy loss	443.11 kWh	235.56 kWh
Efficiency	**97.96 %**	**98.88 %**
Mean station power	723.03 kW	702.69 kW
Maximum station power	**3.35 MW**	**1.55 MW**

Station self-consumption analysis

To finish with the station and fleet analysis, and supposing that the charging station is located on the installations of a delivery or logistics enterprise such as GLO, apart from the charging demand there is also a local consumption. Additionally, it is becoming quite common to count on a renewable local generation to supply or at least reduce the self-energy demand. In this section, the effect of integrating the three power profiles (charging demand, installation demand and renewable generation) is evaluated, to introduce self-consumption and energy cost savings concepts.

The charging demand peak power level reached 1.55 MW, therefore, local demand and generation power levels were adjusted in a similar scale. For that, PV energy source is considered, with a typical generation profile of 10 MWp. For the local demand, some industrial demand profiles were aggregated reaching the 4.13 MWp and 23.62 GWh/year. As Figure 12 shows, both power demands (local and charging demand) and generation are shown, as well as the total balance, which results in energy being purchased when local generation cannot meet the whole demand, and an energy surplus being injected to the grid when there is excess generation.

This project has received funding from the European Union's HORIZON EUROPE research and innovation programme under grant agreement No. 101096028. The content of this publication is the sole responsibility of the Consortium partners listed herein and does not necessarily represent the view of the European Commission or its services.

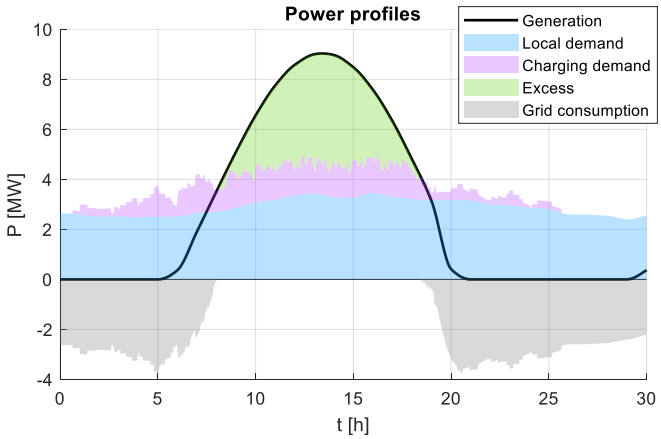

Figure 12: Station self-consumption analysis with local demand, charging demand and PV generation.

In this scenario, energy cost calculations must be adapted to account for both grid-imported energy and exported excess energy. The fixed energy cost (access toll) applies only to energy consumed from the grid, not to locally generated energy or excess energy injected into the grid. Additionally, this excess energy injection is compensated at a reduced rate. However, variable energy term would never result in a payment to the consumer, limiting the total variable energy cost to zero when excess energy is too high.

To reflect this, both fixed and variable energy costs are recalculated based on power balance at each time interval. The cost per EV is then determined proportionally according to its share of total demand. When local generation exceeds consumption, the surplus is factored into the variable cost with a 50% price reduction. Ultimately, the total energy cost is the sum of these adapted fixed and variable components, calculated at either the station or EV level.

As a result, energy and power cost are calculated as shown in Figure 13. The more significant cost corresponds to energy demand, by both local and charging demands. At the same time, delay cost split in time can also be observed. In comparison to energy and delay, power cost is low.

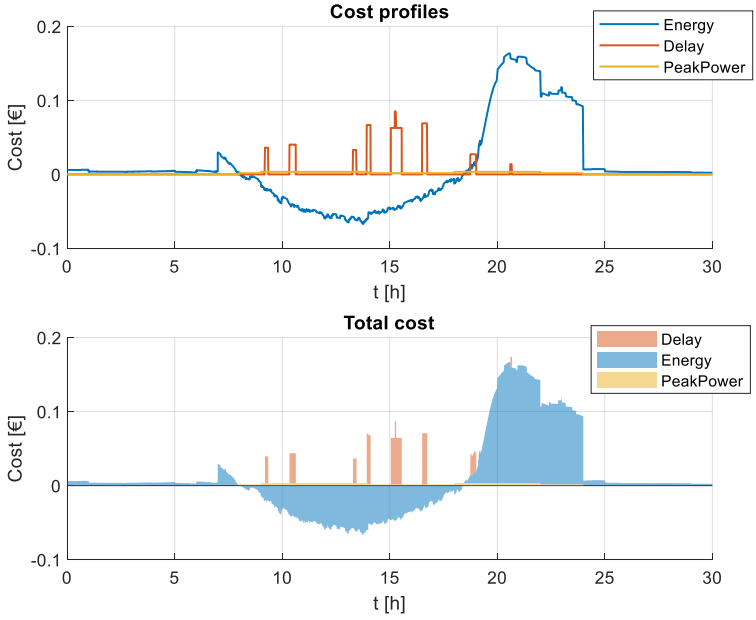

Figure 13: Station energy and power cost evaluation with local demand, charging demand and PV generation.

This project has received funding from the European Union's HORIZON EUROPE research and innovation programme under grant agreement No. 101096028. The content of this publication is the sole responsibility of the Consortium partners listed herein and does not necessarily represent the view of the European Commission or its services.

As a result, a self-consumption ratio of 66.35 % (which means that 66.35 % of the generated energy is locally consumed) and a self-sufficiency of 50.79 % (which means that 50.79 % of the demand is supplied by local generation) is reached, with a cost saving of 81.85 %, with respect to a non-local-generation scenario.

2.1.4 Conclusions

In this study an efficient SVC strategy and a SFC strategy are proposed and evaluated, demonstrating promising results in terms of energy efficiency, system performance, and practicality for real-time implementation.

For the SVC strategy, it was proved that current modulation can increase the efficiency of the charging process. This improvement depends on battery technology and the corresponding resistive behavior. Furthermore, current modulation reduces peak power, which contributes to mitigating battery degradation. Although, the extension of the charging time reduces the C-rate and consequently the power loss, this is not always feasible. Hence, the developed strategy optimizes both power losses and charging time.

This efficient SVC is then used for the SFC where charging scheduling is defined. It is true that the defined scenario (10 chargers and 120 electric HDVs) leads to a high usage of chargers, where fast charging results more effective to minimize delays, but this would cause a higher degradation in the battery system and would increment the peak power demand. By applying efficient charging SVC, more than a 50 % of power peak reduction is obtained, benefiting both infrastructure and power cost impact.

In the defined scenarios, delay cost is the most significant economic factor when scheduling, since energy and power costs remain relatively stable even if scheduling is modified, which makes delay reduction the priority. In the criteria comparison, the departure criteria turned out to be the more convenient strategy, because it obtains the lower delay values. Moreover, it was proved that this delay could even be completely avoided by a later scheduling and SVC profile correction step, in which delays were limited and possible charging time extensions applied to maximize both chargers and available time usage while improving charging performance and efficiency. When charging flexibility is high, adjusting the power profiles of individual vehicles can provide overall system benefits. Even advanced concepts like V2G could be explored. This could increase self-consumption and self-sufficiency ratios and reduce energy costs. However, this does not result interesting in the defined scenario, since minimizing delays remains the primary objective.

In the analysis of the SFC, the results provide insights into determining the optimal number of chargers for a given station. If optimal number of charging point is desired, then scheduling of vehicles becomes important since chargers are highly used throughout the day. If chargers are underutilized, scheduling may not be necessary, and the best approach would be to charge vehicles as soon as they arrive to avoid delays. This study could help also on optimizing number of charging points to balance installation costs and delay time.

Additionally, the savings to be obtained by including renewable energy sources depends on the local demand and generation profiles, but it can be significant as shown in the example scenario, reaching 81.85 % of savings in energy and power costs.

Anyways, the potential for optimization in this field is significant, since multiple factors are involved. In this study, an efficient charging strategy was developed that does not substantially affect charging time, as well as a straightforward yet effective scheduling, making the strategy practical for real-time use.

As a next step, the proposed strategy could be integrated into a real-time operational environment. For this purpose, the development of dedicated software and an intuitive interface for station or fleet management has been started. This tool would allow monitoring of daily operations, and include the implementation of the SVC

This project has received funding from the European Union's HORIZON EUROPE research and innovation programme under grant agreement No. 101096028. The content of this publication is the sole responsibility of the Consortium partners listed herein and does not necessarily represent the view of the European Commission or its services.

strategy, which could be defined either by the station or fleet manager, or even by the end-user on-site. Ultimately, moving from simulation to a real-time management system would make the proposed approach applicable in real-world conditions, supporting more efficient and sustainable electric fleet operations.

2.2 Task 5.3

2.2.1 Aging models

CID built a set of aging models that are integrated into IFPEN's fleet management tools. These models are based on the eBS69 battery, which will be integrated into the vehicles and will be in operation in the demonstration phase. The models are the following:

- Model 1: With external temperature and discharge current as input data, the model returns an estimation of the aging rate of the battery under those conditions. Figure 14 depicts the general structure of the model, as discussed with IFPEN.

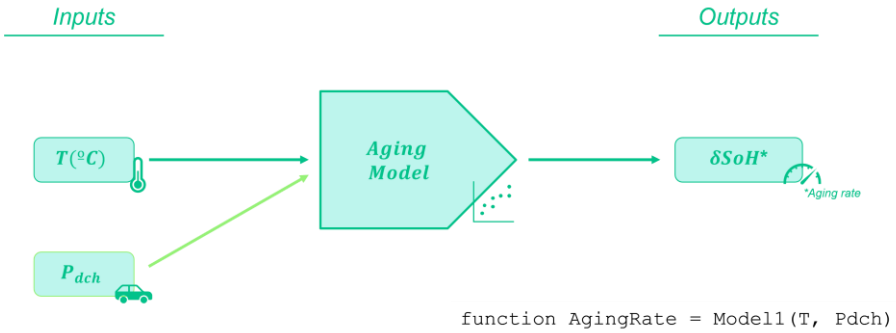

Figure 14: Diagram for the structure of model 1.

- Model 2: With charge-related input data (SoC before charge, SoC after charge and charge power), the model returns an estimation of the total aging relative to the described charge. Figure 15 depicts the general structure of the model, as discussed with IFPEN.

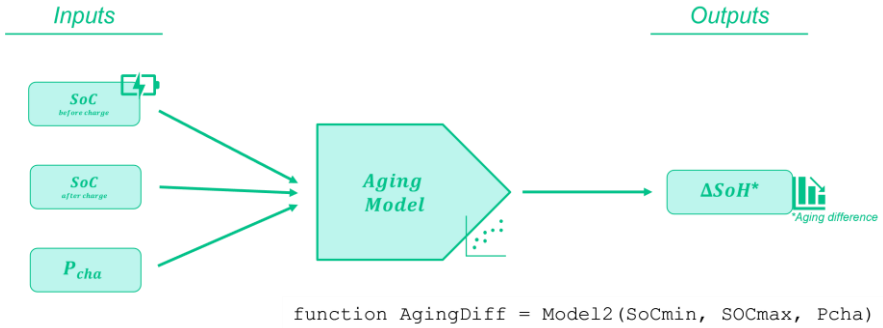

Figure 15: Initial diagram for the structure of model 2.

IVECO has provided CID with data to build these models. Aging curves were given for two different cases. The aging rates of these curves were calculated, and additional data was extracted from the literature for cells with similar chemistry. The slope of the linear regression curve is considered as the aging rate of a degradation curve.

The cells from the literature had faster aging trends than the ones from the data provided by IVECO. To account for this, a dummy variable was considered during the optimization of the models ($\gamma = 1$ if the data comes from IVECO and $\gamma = 0$ if it comes from the literature) together with an elongation factor. It is assumed that all variables have a representative impact on the cells' aging, regardless of differences in their structure. This approach allows for the influence of the stress factors on the shorter-lifespan literature cells to be extrapolated over to the longer-lifespan eBS69 battery cells.

This project has received funding from the European Union's HORIZON EUROPE research and innovation programme under grant agreement No. 101096028. The content of this publication is the sole responsibility of the Consortium partners listed herein and does not necessarily represent the view of the European Commission or its services.

In Table 6, the values for the aging factors are displayed for every available case. It can be noted that DOD is used instead of the minimum SOC value for the cycle. Given the maximum SOC value, the transformation is immediate. In Figure 16, the difference in the aging rates between the aging curves from the literature (cases 1 to 17) and those from IVECO (cases 18 and 19) is portrayed. Current is also used instead of power.

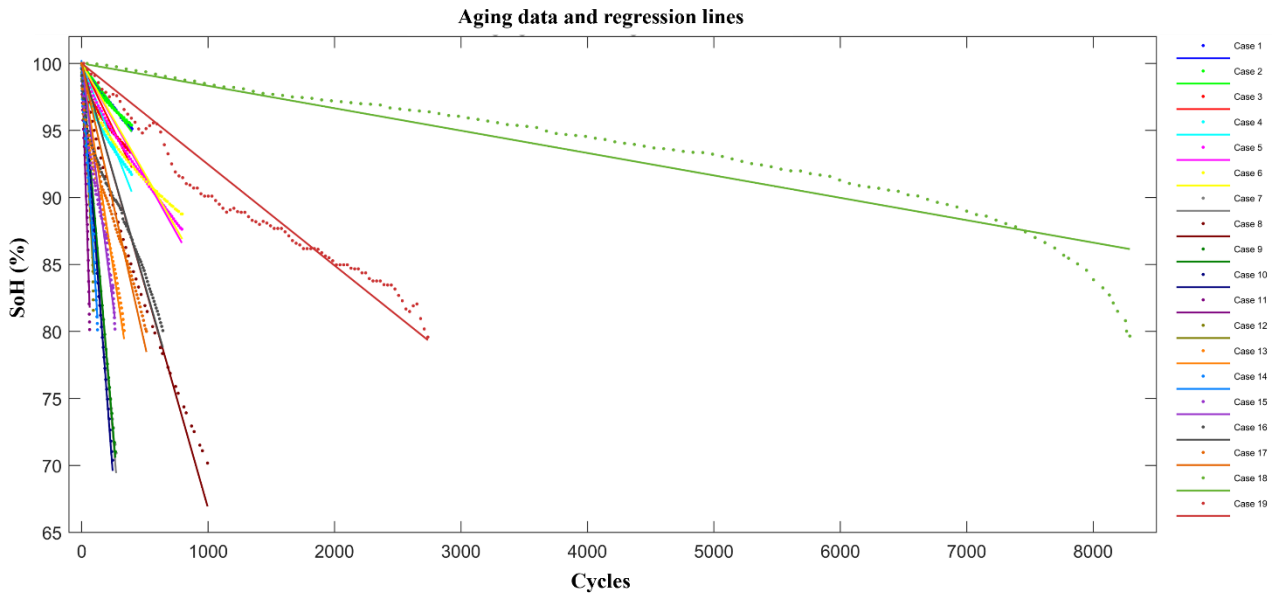

Figure 16: Aging curves of all available data (dotted) and linear regression curves for each case.

Table 6: Degradation variable values for the aging curves available to CID. Cases 1 to 17 refer to data from the literature and cases 18 and 19 refer to data provided by IVECO. The table highlighted with a red line contains degradation factors relevant to model 1, while the table highlighted with a green line contains degradation factors relevant to model 2.

Case Nº	T (ºC)	Idch (C-rate)	Icha (C-rate)	SoC max. (%)	DoD (%)	Literature data / Real data (γ)
1	35	.75	.75	30	20	Literature ($\gamma = 0$)
2	35	.75	.75	50	20	Literature ($\gamma = 0$)
3	35	.75	.75	70	20	Literature ($\gamma = 0$)
4	35	.75	.75	90	20	Literature ($\gamma = 0$)
5	35	.75	.75	50	40	Literature ($\gamma = 0$)
6	35	.75	.75	70	40	Literature ($\gamma = 0$)
7	35	.75	.75	90	40	Literature ($\gamma = 0$)
8	35	.75	.75	70	60	Literature ($\gamma = 0$)
9	35	.75	.75	90	60	Literature ($\gamma = 0$)
10	35	.75	.75	90	80	Literature ($\gamma = 0$)
11	0	1	1	100	100	Literature ($\gamma = 0$)
12	10	1	1	100	100	Literature ($\gamma = 0$)
13	25	1	1	100	100	Literature ($\gamma = 0$)
14	0	1	.5	100	100	Literature ($\gamma = 0$)
15	10	1	.5	100	100	Literature ($\gamma = 0$)
16	25	1	.5	100	100	Literature ($\gamma = 0$)
17	40	1	.5	100	100	Literature ($\gamma = 0$)
18	25	1	1	100	100	Real ($\gamma = 1$)
19	45	1.5	1.5	100	100	Real ($\gamma = 1$)

This project has received funding from the European Union's HORIZON EUROPE research and innovation programme under grant agreement No. 101096028. The content of this publication is the sole responsibility of the Consortium partners listed herein and does not necessarily represent the view of the European Commission or its services.

The available cases differ in both the variables to consider for model 1 and in the ones for model 2. To consider this, CID has constructed a single model that covers all degradation factors. Models 1 and 2 can then be built based on it. Figure 17 displays a diagram for this general model.

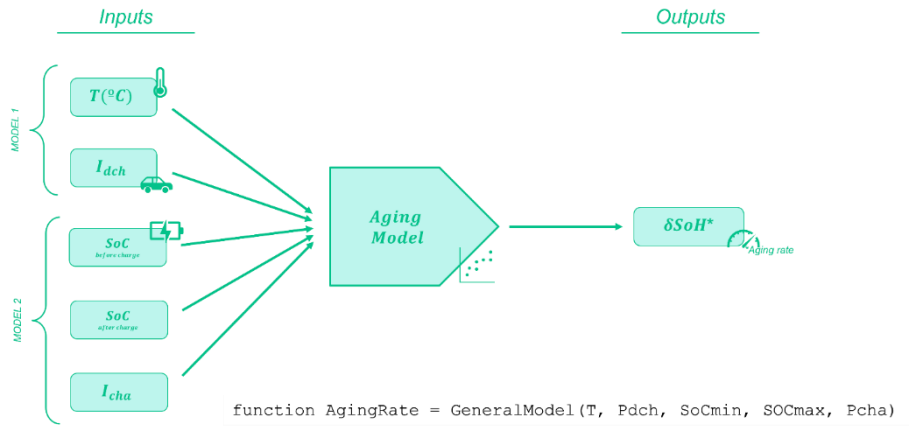

Figure 17: Diagram for the general model considering both variables from model 1 and model 2 as inputs.

The model is a non-linear regression model. To obtain its expression, a previous analysis was done on the effect of each of the model inputs. Figure 18 and Figure 19 show the aging of each case from the literature against every input variable throughout multiple 2D scatter plots.

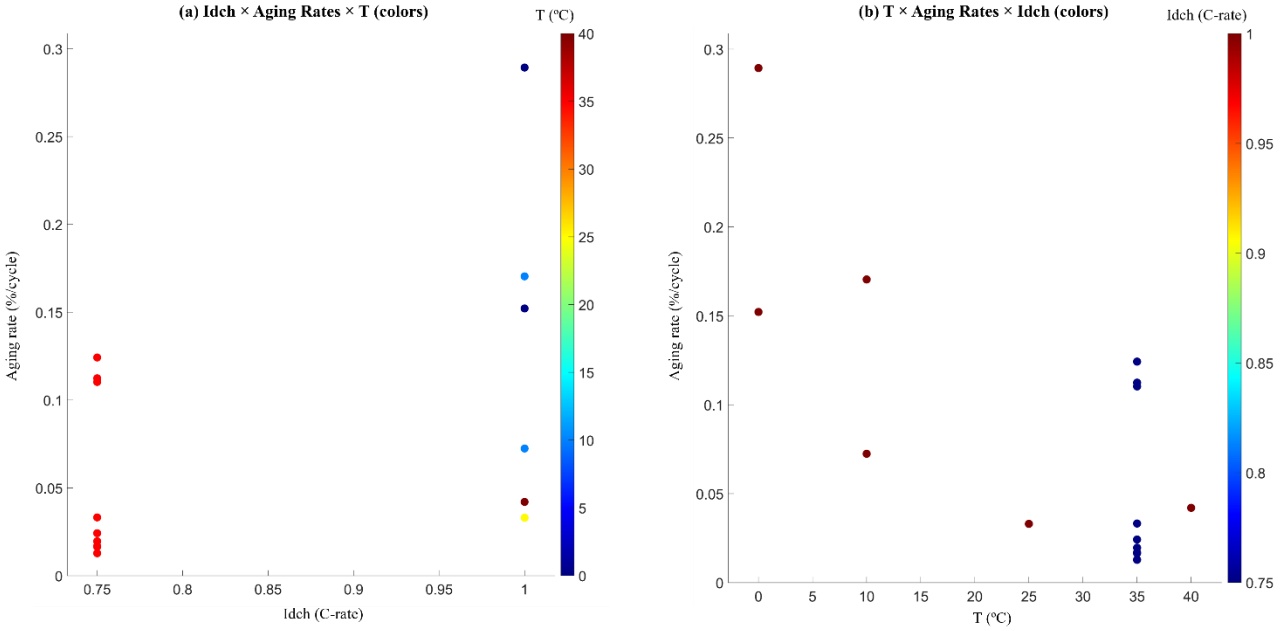

Figure 18: Input variables for model 1 against the aging rates of the curves from the literature.

This project has received funding from the European Union's HORIZON EUROPE research and innovation programme under grant agreement No. 101096028. The content of this publication is the sole responsibility of the Consortium partners listed herein and does not necessarily represent the view of the European Commission or its services.

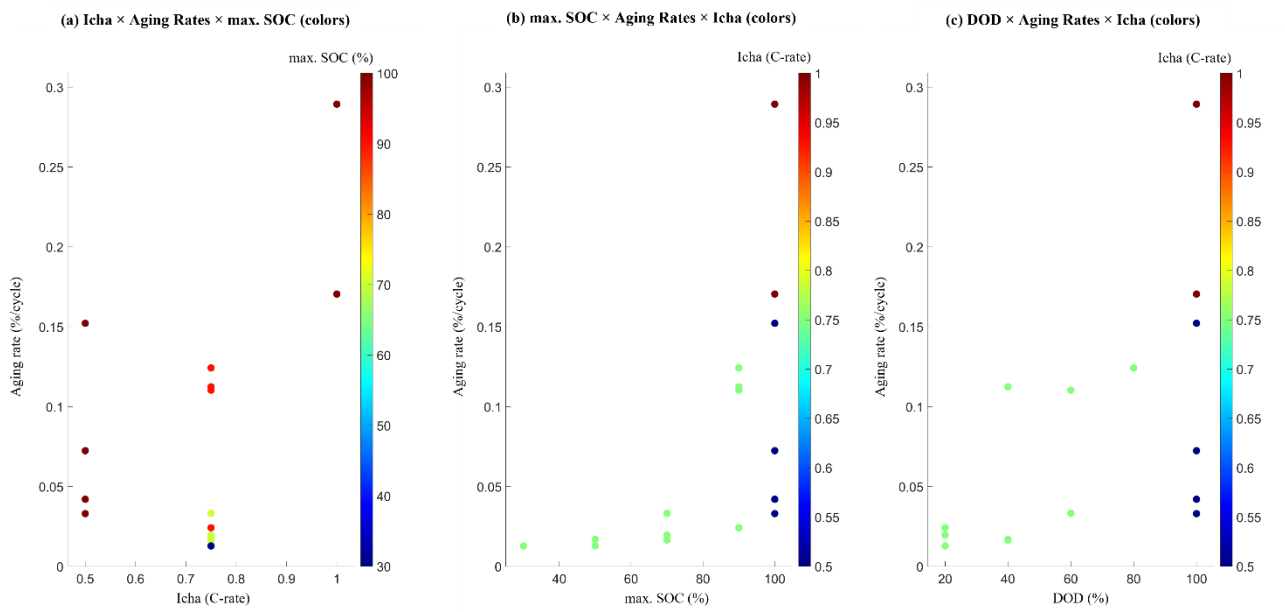

Figure 19: Input variables for model 2 against the aging rates of the curves from the literature.

Through thorough inspection, testing, and CID's expertise in aging models, the following is the expression selected for the general model:

$$AgingRate = \beta_0 \cdot (1 - \beta_1 \cdot \gamma) \cdot A(T) \cdot B(I_{dch}) \cdot C(I_{cha}) \cdot D(SOC_{max}) \cdot E(DOD) \quad (7)$$

With A, B, C, D and E being the functions that describe the effect of each aging factor on the aging rate of the cells:

$$A(T) = \begin{cases} (T \leq \beta_2) & (1 + \beta_3 \cdot \beta_2^2) - (2 \cdot \beta_3 \cdot \beta_2) \cdot T + \beta_3 \cdot T^2 \\ (T > \beta_2) & (1 + \beta_4 \cdot \beta_2^2) - (2 \cdot \beta_4 \cdot \beta_2) \cdot T + \beta_4 \cdot T^2 \end{cases} \quad (8)$$

$$B(I_{dch}) = I_{dch}^{\beta_5} \quad (9)$$

$$C(I_{cha}) = I_{cha}^{\beta_6} \quad (10)$$

$$D(SOC_{max}) = \left(\frac{SOC_{max}}{100}\right)^{\beta_7} \quad (11)$$

$$E(DOD) = \log(DOD + \beta_8) \quad (12)$$

Once the parameters have been estimated, the results of the model are shown. Table 7 displays the results of the model for the data provided by IVECO, while Figure 20 contains a visual representation of these results. Figure 21 shows the results of the model for a sample of the aging curves from the literature, which is not representative of the real aging rates of eBS69 battery cells but shows that the model is able to appropriately reflect the effects of the stress factors.

Table 7: Aging rates for the aging curves provided by IVECO, as well as the aging rates estimated by the model and their absolute and relative errors.

Case Nº	Aging Rate (%/cycle)	Estimation	Absolute Error	Relative Error (%)
18	0.00167126	0.00170787	3.6609E-05	2.19050484
19	0.00754074	0.00753244	8.3005E-06	0.11007501

This project has received funding from the European Union's HORIZON EUROPE research and innovation programme under grant agreement No. 101096028. The content of this publication is the sole responsibility of the Consortium partners listed herein and does not necessarily represent the view of the European Commission or its services.

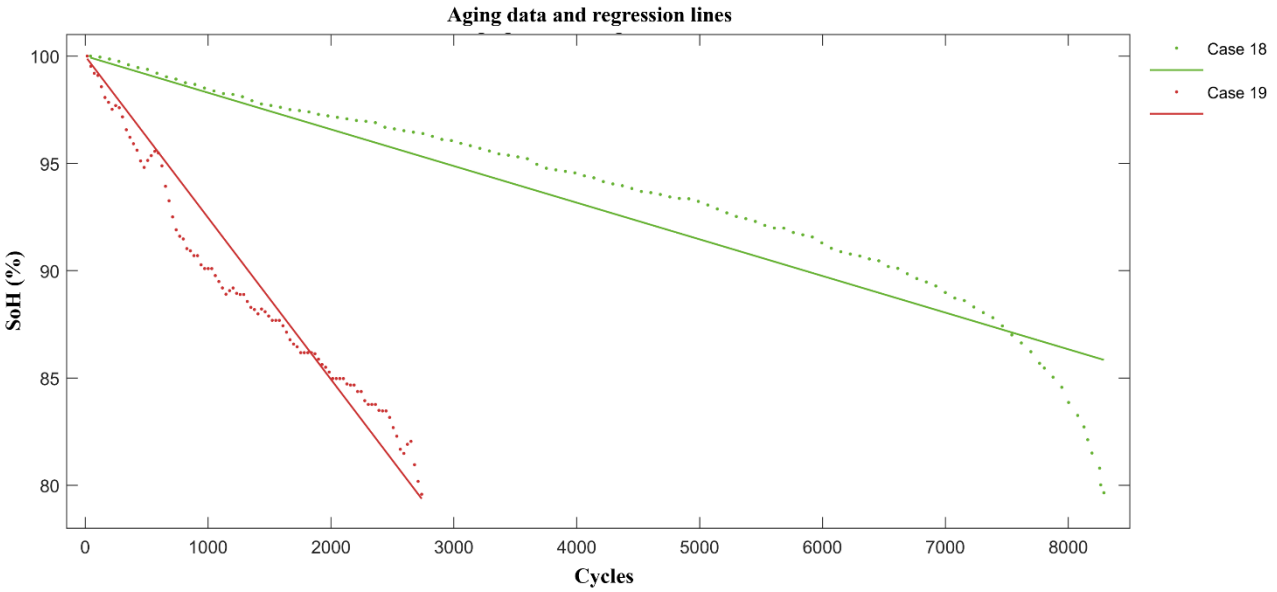

Figure 20: Aging curves (dotted) and linear regression curves estimated by the aging rate model for the data provided by IVECO.

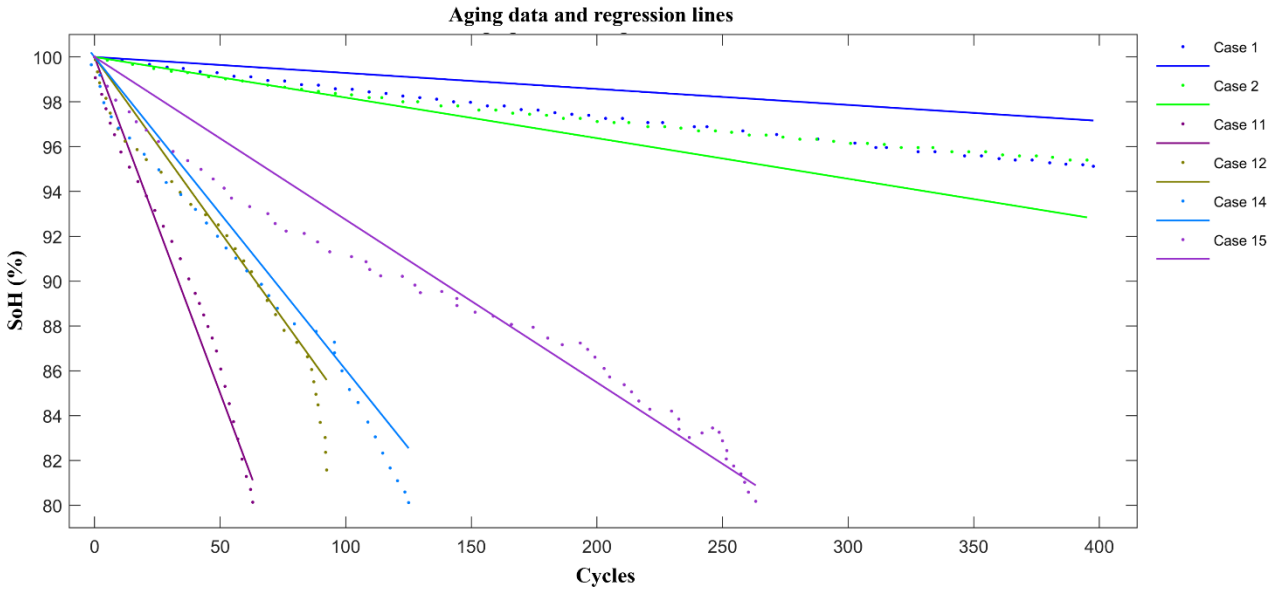

Figure 21: Aging curves (dotted) and linear regression curves estimated by the aging rate model for data from the literature.

With this estimator as the general model, model 1 and model 2 were constructed. For model 1, $max.SOC$ was fixed at 100 % and DOD at 100 %. For model 2, T was fixed at 25 ºC. Both models assume that I_{dch} and I_{cha} take the same values. γ is always fixed to 1.

For model 2, minimum SOC values are considered as inputs for consistency with the initial model proposal. Another adjustment was made, as the general model returns the aging rate as an output, not the aging difference for the defined charge. By assuming that the relation between the cycles and the aging of the cells is linear, it can be deduced that the aging of a cell during a single FEC would be equal to its aging rate. However, on different SOH levels, a single charge will not account for the same amounts of FECs.

The calculations for the FECs from the SOH of the battery have also been implemented in the second model. To do this, the SOH has been added as an input. If this is not available, it can be fixed at 100%.

This project has received funding from the European Union's HORIZON EUROPE research and innovation programme under grant agreement No. 101096028. The content of this publication is the sole responsibility of the Consortium partners listed herein and does not necessarily represent the view of the European Commission or its services.

All models interpolate inside the ranges of each of their input variables, but they do not extrapolate. If given values outside their definition range, saturation will occur; the closest value in range will be used for the calculations instead. Figure 22 and Figure 23 serve as verification for model 1 and model 2, which have been designed with an extended range for every variable for better visualization of saturation. It should be noted that SOH is fixed at 100% in Figure 23.

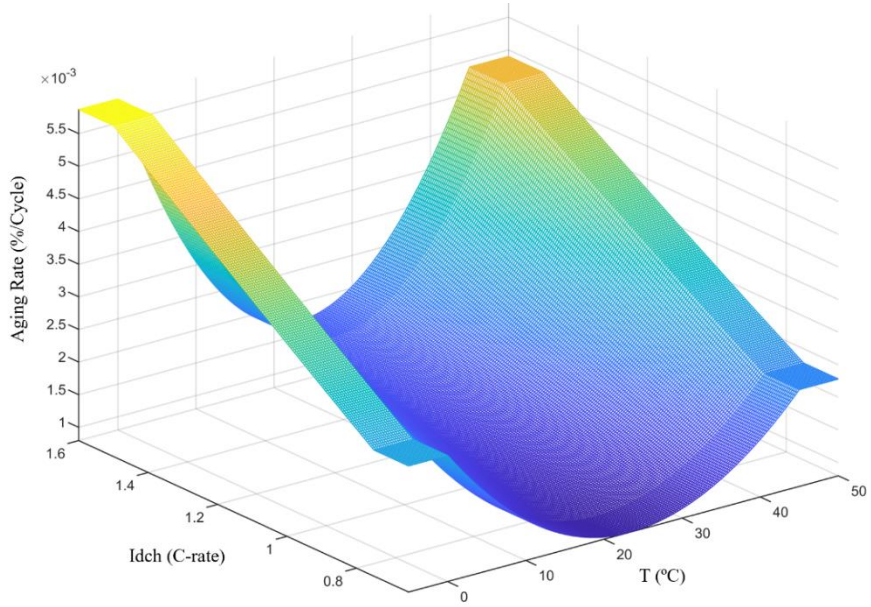

Figure 22: Saturated outputs from model 1 against temperature and discharge current values.

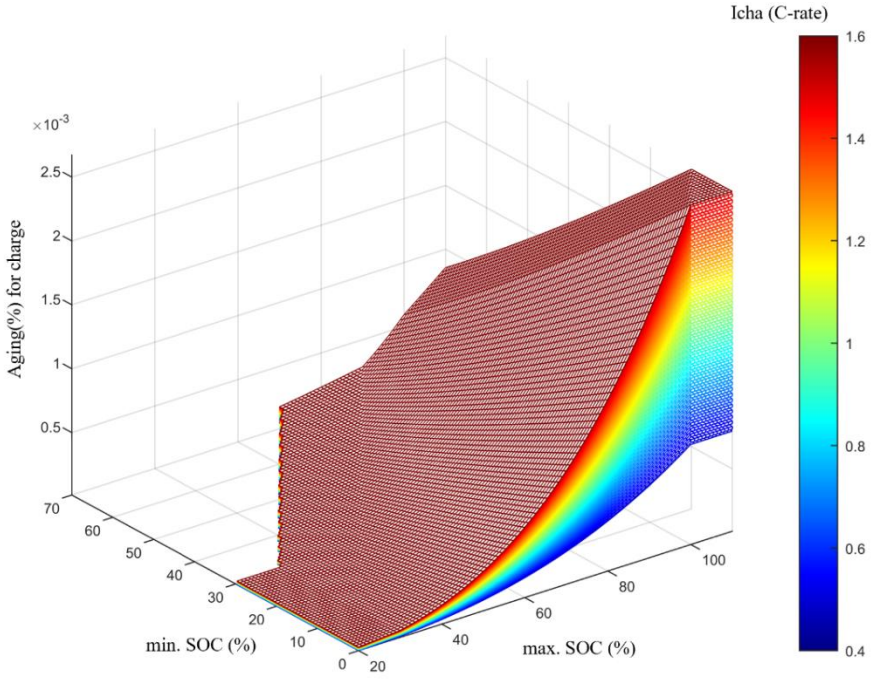

Figure 23: Saturated outputs from model 2 against minimum and maximum SOC values and charge current values.

The two required models and the general model were provided to IFPEN as MATLAB P-files, along with a guide on how the models work and how to call the MATLAB functions.

This project has received funding from the European Union's HORIZON EUROPE research and innovation programme under grant agreement No. 101096028. The content of this publication is the sole responsibility of the Consortium partners listed herein and does not necessarily represent the view of the European Commission or its services.

3 Eco strategies

One of the main obstacles for the widespread adoption of e-HDV is range anxiety, as e-HDVs have limited battery capacity and rely on a still-developing charging infrastructure. Additionally, factors such as charging time, energy consumption variability, and route planning complexity contribute to hesitancy among fleet operators and logistics companies [14]. In this context, optimizing trip planning and user driving for e-HDVs plays a crucial role in facilitating this transition. Providing efficient, well-structured trip plans and driving advice help mitigate range anxiety, optimize energy consumption, and minimize operational costs, reinforcing the perception that adopting electric solutions is both feasible and economically advantageous.

Eco-strategies for e-HDV presented in this deliverable are a combination of eco-routing/charging and eco-driving techniques. These strategies work together to enhance the energy efficiency, cost-effectiveness, and overall sustainability of vehicle trips and have been subject of past study in the CEVOLVER and LONGRUN European projects in the context of e-LDV and ICE HDV, as documented in [15, 16]. While eco-charging focuses on planning the best combination of route and charging events, eco-driving involves adapting driving behavior and vehicle operation to minimize energy consumption. The global architecture is illustrated in Figure 24. The eco-charging strategy consists of a planning process aimed at selecting the most favorable trip plan for a user traveling from an origin to a destination. This planning considers constraints posed by the route and charging infrastructure, traffic conditions, and user preferences. The objective is to determine a trip plan that minimizes a weighted combination of energy consumption, travel time, and economic cost, while adhering to the feasibility constraints imposed by charging infrastructure and vehicle characteristics. From an external characterization perspective, the input/output behavior of the eco-charging strategy can be described as follows:

Input

- A set of user preferences (U), such as priorities for energy, cost, or time savings, and safety constraints like maintaining minimum SOC levels.
- Data about the charging network infrastructure (N), including location, type, availability, charging speed, and cost of charging stations along the potential routes
- A vehicle's model (M), based on physical characteristics, including mass, battery parameters, drivetrain efficiency, and regenerative braking capacity

Output

- A route model (R), accounting for road conditions, such as terrain, road slope, surface type, traffic data, and weather.
- An optimal trip plan (TP), consisting of: the geographical route to be followed; the charging plan, specifying where and how long charging sessions should take place ; a driving-style in terms of average speed to be adopted along different segments of the route.

Algorithm Structure

1. **Itinerary Calculation**: Various potential routes are computed using a GIS-based service, considering the origin, destination, and user constraints.
2. **Route Contextualization**: Each route is analyzed to extract road characteristics such as speed limits, traffic signs, and average speeds.
3. **Graph Formulation**: A graph model is constructed, integrating road data with charging infrastructure. Nodes represent locations ; links represent segments with travel/traffic attributes.

This project has received funding from the European Union's HORIZON EUROPE research and innovation programme under grant agreement No. 101096028. The content of this publication is the sole responsibility of the Consortium partners listed herein and does not necessarily represent the view of the European Commission or its services.

4. **Profile Generation**: For each route segment, realistic speed profiles are computed, factoring in vehicle behavior and infrastructure constraints. Using the speed profiles, energy consumption can be calculated based on a consumption model.

5. **Graph extensions**: The graph is extended to a hypergraph, combining spatial information with SOC levels. Nodes and edges reflect both driving and charging states and decisions.

6. **Graph Optimization**: A shortest-path search is performed on the hypergraph to produce the optimal route and charging plan, minimizing a weighted cost function based on energy, time, and economic factors.

The eco-driving strategy focuses on optimizing how the vehicle should be precisely driven to minimize energy consumption during the trip. Unlike eco-charging, which emphasizes when and where to recharge, eco-driving aims to reduce energy use through efficient speed modulation, acceleration control. The eco-driving strategy can be characterized by the following inputs and outputs:

Input

- A vehicle model (M) identical to the one used by the eco-charging stage
- The route model (R) obtained from the eco-charging output
- The optimal trip plan (TP) obtained from the eco-charging output

Output

- A detailed speed trajectory (SP) along the planned route.

Algorithm Structure

7. **Initial Solution Generation:** realistic speed and consumption profiles are generated for each segment, based on the constraints indicated by the trip plan TP over the route R, and using the vehicle model M
8. **Speed Trajectory Optimization:** For each segment, an optimal speed profile that minimizes energy consumption is calculated.

The remainder of the Part 3 is organized as follows. In Section 3.1 we present the hardware and software architecture. The different models are then introduced: the routing model in Section 3.2, the e-HDV and driver model in Section 3.3, and the charging network model in Section3.4. The theoretical framework for the eco-charging and eco-driving strategies is provided in Section 3.5 and Section 3.6 respectively. Finally, simulation results for both strategies are presented in Section 3.7.

This project has received funding from the European Union's HORIZON EUROPE research and innovation programme under grant agreement No. 101096028. The content of this publication is the sole responsibility of the Consortium partners listed herein and does not necessarily represent the view of the European Commission or its services.

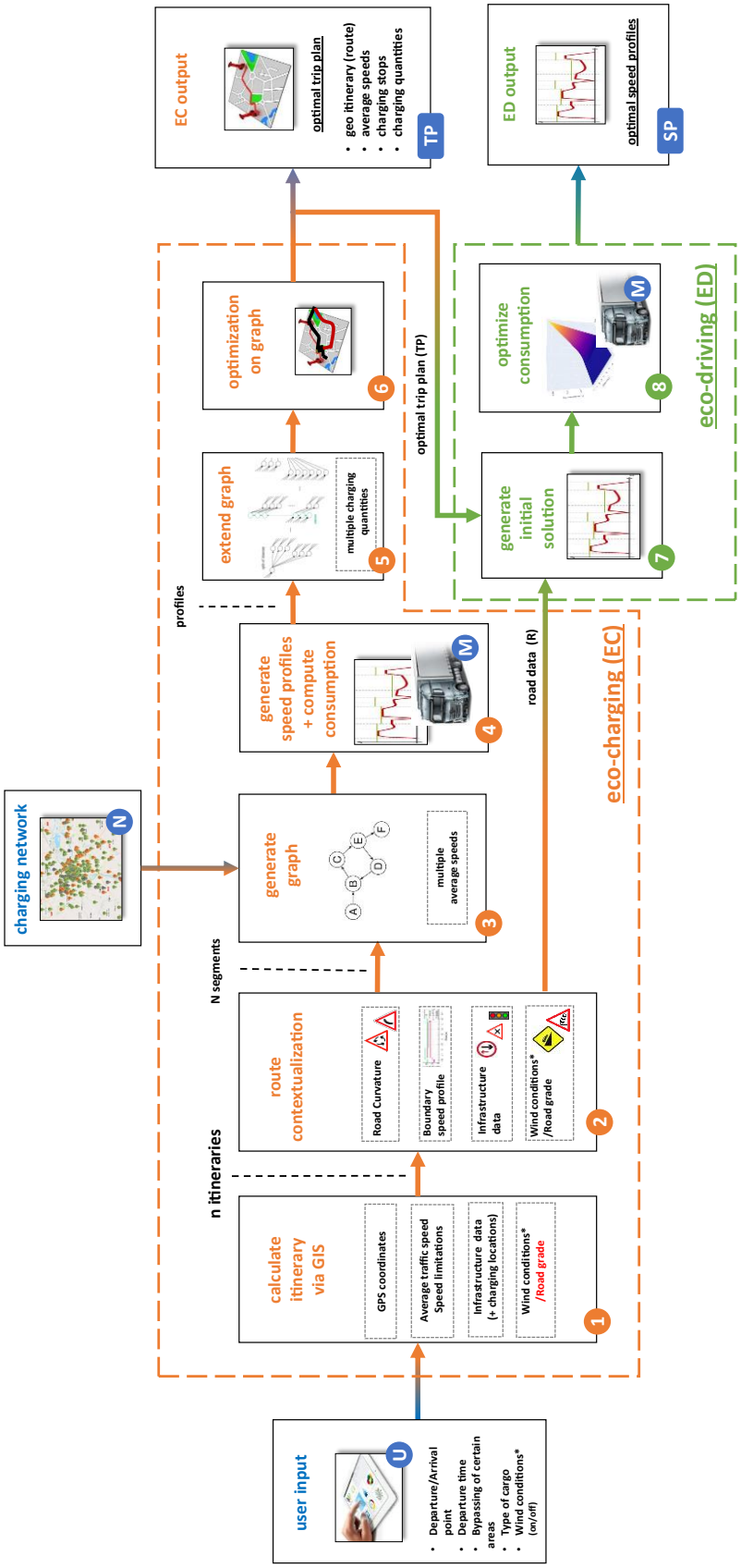

Figure 24: Global architecture of the eco-strategies.

This project has received funding from the European Union's HORIZON EUROPE research and innovation programme under grant agreement No. 101096028. The content of this publication is the sole responsibility of the Consortium partners listed herein and does not necessarily represent the view of the European Commission or its services.

3.1 Hardware and software architecture

The hardware architecture, as depicted in Figure 25, illustrates the integration of onboard and remote components. This approach aims to optimise energy efficiency and operational effectiveness across the fleet, aligning closely with the project's overarching goals of sustainability and smart mobility solutions. It was decided to use the IVECO hardware (telematic unit and infotainment system) to host the LT HVI and IFPEN algorithms. The telematic unit is an automotive grade embedded ARM device, the infotainment is an Android device.

The Eco-charging/Eco-driving (EC/ED) controller and the Eco-driving algorithm will access all PCM board services dealing with the middleware service by gRPC protocol calls and service specific APIs.

These services include:

- Retrieval of CAN and sensors data
- Communication with the Android frontend (this feature relies on a dedicated software of the telematic unit that works as bridge towards the infotainment)
- Web access

The Android frontend on the infotainment will communicate with the EC/CD controller and eco-driving through a specific API developed by IVECO.

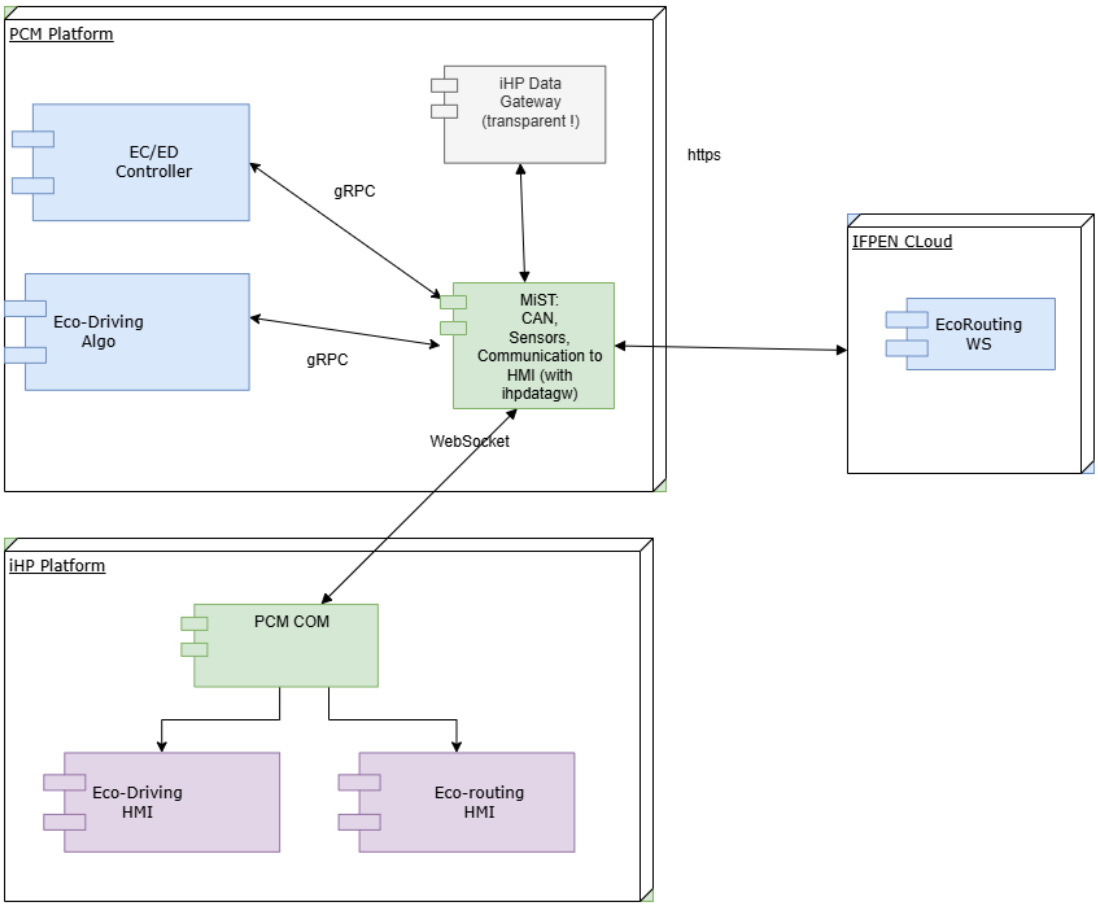

Figure 25: Hardware architecture for integrating both onboard and remote functionalities

This project has received funding from the European Union's HORIZON EUROPE research and innovation programme under grant agreement No. 101096028. The content of this publication is the sole responsibility of the Consortium partners listed herein and does not necessarily represent the view of the European Commission or its services.

EC/ED controller is responsible for:

- calling the Eco-routing web service hosted by the IFPEN cloud (Figure 26)
- processing the results and sending them to the HMI eco-routing (Figure 26)
- considering the CAN signals and calling the eco-driving algorithm. (Figure 27)
- sending the eco-driving results to the HMI eco-driving (Figure 27)

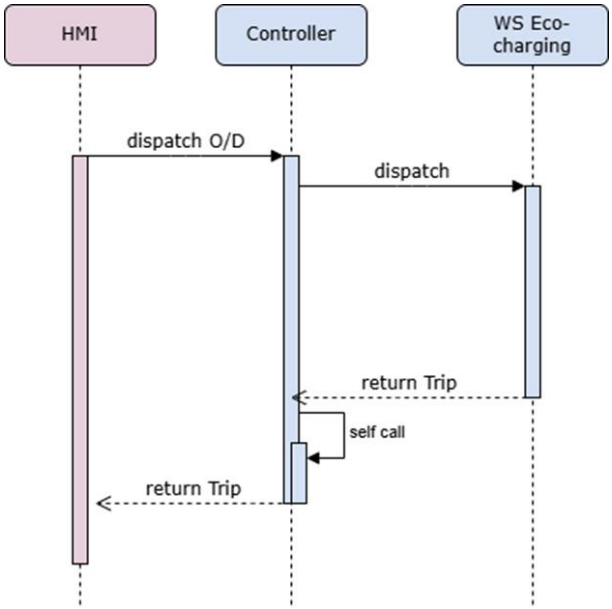

Figure 26: Eco-charging sequence diagram

EC/ED controller retrieves the following vehicle signals form the CAN and provides them to the eco-driving:

- GPS
- Road curvature
- Front axle speed
- Tachograph vehicle speed
- Battery remaining charge
- Gross combination vehicle weight
- Distance to forward vehicle
- Speed of forward vehicle

This project has received funding from the European Union's HORIZON EUROPE research and innovation programme under grant agreement No. 101096028. The content of this publication is the sole responsibility of the Consortium partners listed herein and does not necessarily represent the view of the European Commission or its services.

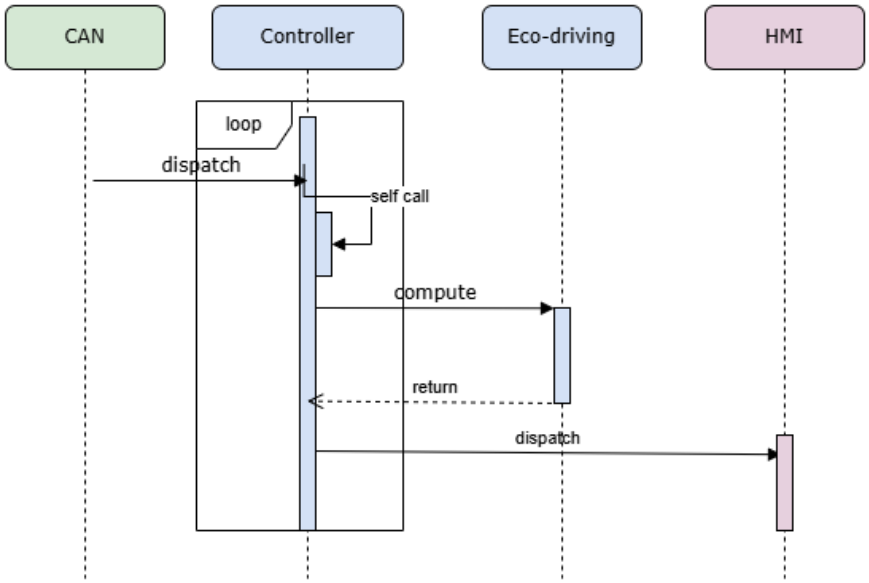

Figure 27: Eco-driving sequence diagram

3.2 Route model

To model routing possibilities, we make use of a GIS, typically a cloud-based platform capable of generating n alternative itineraries between a given origin x_0 and destination $x_\star$, at a specified departure time, with the option of including intermediate waypoints. Each itinerary i is described as an ordered list of waypoints $N^i = \{x_0, \dots, x_p^i, \dots, x_\star\}$, where each waypoint $x_p^i = (lon_p^i, lat_p^i)$ consists of a longitude–latitude pair, both represented by real numbers.

In addition to this geospatial trace, the GIS system provides a structural segmentation of the route, identifying a subset of waypoints $X^i \subset N^i$, and a corresponding set of directed links $\mathcal{E}^i$, each representing a road segment between consecutive waypoints. This segmentation relies on the functional classification of roads—differentiating major highways, arterial roads, and minor urban streets—and accounts for further infrastructure characteristics.

Multiple itineraries can share some waypoints, revealing overlaps where different routes follow the same physical road. From this, we can construct an initial graph $G_0(X_0, E_0)$, where $X_0 = \bigcup_i X^i$ and $E_0 = \bigcup_i E^i$ represent the full set of nodes and edges, respectively. The GIS metadata enriches this graph: each node $x_j \in \mathcal{X}_0$ may be associated with a positive integer z_j, indicating the presence of traffic infrastructure (e.g., lights or signage) at that location. Meanwhile, each edge $(j,k) \in E_0$, connecting two waypoints, carries three key attributes: the legal speed limit $\bar{V}_{jk}$, the average traffic speed under normal conditions V_{jk}^{avg}, and the current traffic speed V_{jk}^{tr}.

An essential step in route modeling involves contextualizing these raw data to establish realistic speed constraints for each road segment. Naturally, the maximum allowable speed along a link cannot exceed the legal limit $\bar{V}_{jk}$However, the maximum final speed V_k° to be achieved at node k can be estimated from z_k, according to the classification outlined in the table below.

This project has received funding from the European Union's HORIZON EUROPE research and innovation programme under grant agreement No. 101096028. The content of this publication is the sole responsibility of the Consortium partners listed herein and does not necessarily represent the view of the European Commission or its services.

Table 8: Mapping between infrastructure events z_k and maximum admissible final speed V_k°.

z_k	Condition	Max. Final Speed V_k° (km/h)
0	New speed limit	$\min(\bar{V}_{jk}, \bar{V}_{k\ell})$
1	Traffic light	$\{V_{jk}^{tr}, 0\}$
2	Stop sign	0
3	Give-way	[20, 40]
4	Traffic jam	V_{jk}^{tr}
5	End of traffic jam	V_{jk}^{tr}

While the GIS segmentation helps define speed constraints based on traffic signals and related infrastructure, it does not account for speed reductions necessitated by geometric features like sharp turns or roundabouts. This omission could compromise safety, particularly for heavy-duty vehicles (HDVs), due to excessive cornering speeds. One geometric attribute useful for identifying such features is curvature, which, though not directly available from GIS data, can be reconstructed using distance and bearing calculations.

Consider two consecutive waypoints x_p and x_q. The distance s_{pq} between them can be approximated by projecting the coordinates to a plane and computing their Euclidean distance. The directional bearing β_{pq} can be obtained using:

$$\beta_{pq} = \operatorname{atan2}(X_{pq}, Y_{pq}) \tag{13}$$

with:

$$X_{pq} = \cos(\mathrm{lat}_q) \cdot \sin(\mathrm{lon}_q - \mathrm{lon}_p), \tag{14}$$

$$Y_{pq} = \cos(\mathrm{lat}_p) \cdot \sin(\mathrm{lat}_q) - \sin(\mathrm{lat}_p) \cdot \cos(\mathrm{lat}_q) \cdot \cos(\mathrm{lon}_q - \mathrm{lon}_p). \tag{15}$$

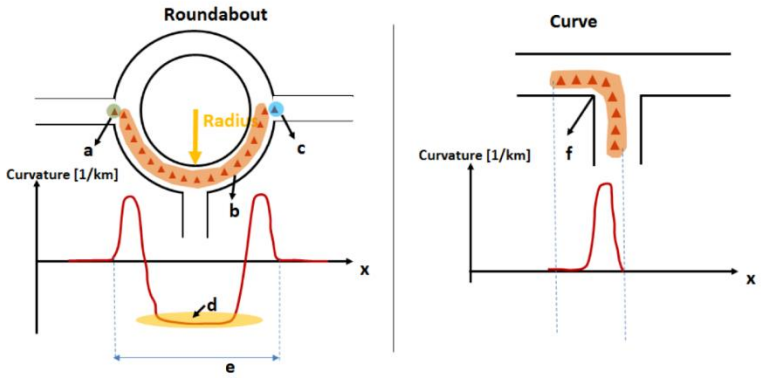

Figure 28: Evolution of the road curvature in a roundabout (left) and a turn (right).

By analysing the variation in curvature, one can distinguish different types of curved segments, see Figure 28 for visual reference. Turns exhibit a gradual and consistent change in direction (f), with nonzero but relatively stable curvature values. Roundabouts, which facilitate continuous traffic flow through a circular intersection, generate characteristic curvature patterns: a smooth change at entry (a) and exit (c), and quasi-constant values within the loop (b, d).

Once curves are detected on a given link $(j,k) \in E$, the minimum safe passage speed can be reasonably approximated [17]. If this speed exceeds the legal speed limit, no correction is necessary. Otherwise, to reflect this constraint, the link can be divided into two sub-links at the point of maximum curvature, where the lowest

This project has received funding from the European Union's HORIZON EUROPE research and innovation programme under grant agreement No. 101096028. The content of this publication is the sole responsibility of the Consortium partners listed herein and does not necessarily represent the view of the European Commission or its services.

traversal speed is expected. The sub-links inherit the legal speed limit V_{jk}, but their final speed constraints differ: the first sub-link ends at the reduced passage speed, while the second resumes with the original final speed.

By applying this curvature-aware correction throughout the network, we derive an extended directed graph $G(X, E)$, where:

- X denotes the set of nodes. Each node $x_j = (\text{lat}_j, \text{lon}_j) \in X$ is associated with an end-speed constraint $\overline{V_j^\circ}$. The origin $j = 0$ and destination $j = \star$ nodes are assigned boundary conditions $\overline{V_0^\circ} = \overline{V_\star^\circ} = 0$, representing initial and final rest states.
- E denotes the set of directed edges, with each edge $(j, k) \in E$ carrying a length L_{jk} and a legal speed limit $\overline{V_{jk}}$.

3.3 e-HDV and driver model

As it will be detailed in Section 3.5 and Section 3.6, a key aspect of the proposed strategies involves determining potential, yet realistic, consumption and charging patterns of the e-HDV under study during both driving and charging processes. The vehicle considered is the 40t e-HDV that assembled by IVECO in the context of the project, in the sequel referred as IVECO BEV. More information about the vehicle layout can be found in Deliverable D2.1 [18].

Consumption and charging patterns for the IVECO BEV during driving can be obtained by first generating realistic speed profiles, which allow to determine reasonable travel time estimates. Once these profiles are established, the corresponding energy consumption can be then calculated based on the vehicle's efficiency. To model these patterns during the charging process, we assume that the energy charged is a multiple of a unit increment, defined as a percentage of the battery's SOC. Given the known energy amount, the required charging time can then be computed as a function of the charger's power rating and the SOC increase from its initial to final value, information that can be obtained from the charging curves of the vehicle.

3.3.1 Generation of Speed Profiles

Generating realistic speed profiles is essential for accurately modeling the energy consumption of an electric heavy-duty vehicle (*eHDV*). To achieve this, we use a high-fidelity vehicle-following model based on a modified version of *Gipps' model* [19]. This approach considers:

- Vehicle dynamics: accounting for acceleration, deceleration, and physical constraints.
- Infrastructure constraints: incorporating road limitations and predefined speed limits along each segment.
- Driver behavior: ensuring a safe and efficient speed trajectory by tracking a reference speed while respecting physical and infrastructure constraints.

A key aspect of this model is the introduction of a "virtual" leading vehicle to enforce speed constraints at the end of a road segment. This mimics a real vehicle gradually slowing down to maintain a safe following distance, thereby ensuring that the e-HDV decelerates smoothly to meet the required speed limit at the end of each segment.

The speed profile for a given road link is defined by the vehicle's position $s(t)$ and velocity $v(t)$ over time t, following the equations:

$$s(t + \epsilon) = s(t) + \epsilon \cdot v(t) \tag{16}$$

This project has received funding from the European Union's HORIZON EUROPE research and innovation programme under grant agreement No. 101096028. The content of this publication is the sole responsibility of the Consortium partners listed herein and does not necessarily represent the view of the European Commission or its services.

$$v(t+\epsilon) = min\,(v_{free}, v_{safe}) \tag{17}$$

with initial conditions $s(0) = 0$, $v(0) = V^{init}$, and:

$$v_{free}(t) = v(t) + 2.5 \cdot a^{max}\epsilon\left(1 - \frac{v(t)}{V^{ref}}\right) \cdot \sqrt{0.025 + \frac{v(t)}{V^{ref}}}, \tag{18}$$

$$v_{safe}(t) = a^{min}\epsilon + \sqrt{\Delta}, \tag{19}$$

where:

$$\Delta = \left(a^{min}\epsilon\right)^2 - 2\,a^{min}[d - s(t)] - \frac{\overline{V^{\circ}}}{a^{min}} - \overline{V^{\circ}} \cdot \epsilon\,, \tag{20}$$

and

- ϵ denotes the driver's reaction time;
- $v_{free}(t), v_{safe}(t)$ denote the speed resulting from a free-flow and safe acceleration behavior;
- d denotes the length of the segment;
- V^{ref} denotes the free-flow speed;
- V^{end} denotes the final speed;
- a^{max}, a^{min} denote the maximum acceleration and deceleration of the vehicle.

Under free-flow behavior, the goal is to increase the vehicle's speed until it reaches the free-flow speed V^{ref}, while under safe acceleration behavior, the goal is to decelerate the vehicle from its current speed to a final speed V^{end}, while covering the remaining part of the link $d - s(t)$.

Solutions to this system must always verify the following constraints:

$$s(T) = d,\ max\big(v(t)\big) \leq V^{ref},\ v(T) = V^{end} \tag{21}$$

where T is the travel time required to cover the segment. To apply this model to the actual route, consider a route link $(j,k) \in E$ connecting node x_j to node x_k. The speed profile for this link must satisfy the following conditions:

$$d = \ell_{jk},\ V^{init} \leq \overline{V_j^{\circ}},\ V^{ref} \leq \overline{V_{jk}},\ V^{end} \leq \overline{V_k}^{\circ} \tag{22}$$

These conditions ensure that the generated speed profile respects the physical constraints of the route and the eHDV's capabilities, ensuring both safety and efficiency.

3.3.2 Vehicle Dynamics Modeling

The eHDV's acceleration is influenced by multiple factors, including the terrain slope and available motor torque. The acceleration behavior is defined as follows :

- Under free-flow conditions, the vehicle attempts to accelerate to reach the target free-flow speed V^{ref}.
- Under constrained conditions, the vehicle decelerates to match the final required speed V^{end} while covering the remaining distance of the road segment.

To model acceleration dynamics accurately, we rely on the maximum torque available at the wheels, which varies with speed and combine this with the nonlinear model of the e-HDV. The maximum wheel torque for the vehicle under study is given in

This project has received funding from the European Union's HORIZON EUROPE research and innovation programme under grant agreement No. 101096028. The content of this publication is the sole responsibility of the Consortium partners listed herein and does not necessarily represent the view of the European Commission or its services.

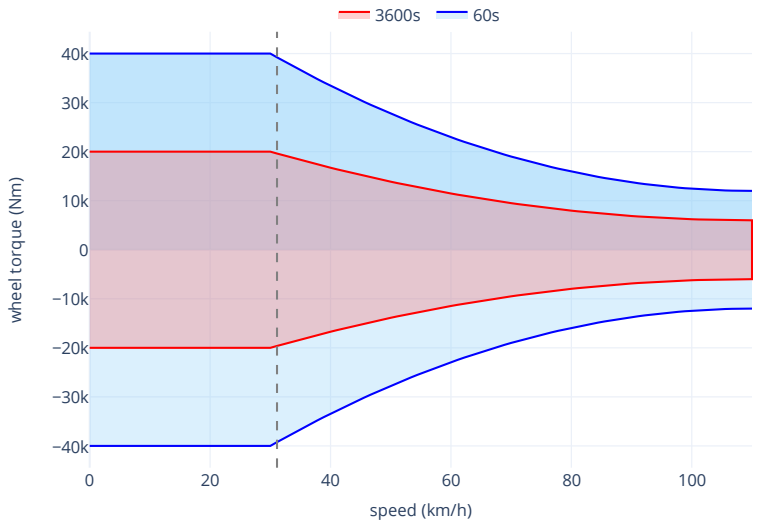

Figure 29: Maximum wheel torque capabilities for the motor mounted on the IVECO BEV as function of the speed.

The equation governing vehicle acceleration is derived from Newton's second law:

$$m \cdot a(s,v) = \frac{T_{wheel}(v)}{r} - F_{res}(s,v) \tag{23}$$

where m denotes the mass, r the tire radius, a the acceleration, and F_{res} the resistive force, while the wheel torque T_{wheel} can be decomposed as follows:

$$T_{wheel} = T_{pwt} + T_{brk} \tag{24}$$

Here, T_{pwt} and T_{brk} represents respectively the powertrain and braking torque. The resistive force F_{res} reads:

$$F_{res}(s,v) = \frac{1}{2} C_d \rho A v^2 + C_r mgcos\,(\alpha) + mgsin\,(\alpha(s)) \tag{25}$$

where the added terms represent respectively aerodynamic drag, rolling resistance, and gravitational forces due to terrain slope $\alpha(s)$, and parameters $C_d, C_d, A, \rho,$ and g correspond to aerodynamic drag coefficient, rolling resistance coefficient, frontal surface of the vehicle, air density and Earth gravity. Using manufacturer data for the maximum torque available at the wheels, $T_{wheel}^{max}\,(v)$, we can compute the physically feasible maximum acceleration:

$$a^{max}\ (s,v) = \frac{1}{m}\left[\frac{T_{wheel}^{max}(v)}{r} - F_{res}(s,v)\right] \tag{26}$$

To substantiate the relevance of considering a^{max} as a variable rather than a constant, we present a comparison in Figure 30 and Figure 31, where speed and torque profiles are generated for an example link of length $L = 1$ km, zero initial speed, i.e., $V_{init} = 0$ km/h, end speed $\bar{V}^{\circ} = 50$ km/h, free-flow speed $V^{ref} = 70$ km/h. These figures illustrate that while a constant maximum acceleration results in a smoother speed profile, the wheel torque generated violates the maximum wheel torque physically realizable by the vehicle. This highlights how the variable acceleration model better captures the impact of terrain slope and vehicle speed on performance, leading to more realistic and physically feasible speed trajectories.

This project has received funding from the European Union's HORIZON EUROPE research and innovation programme under grant agreement No. 101096028. The content of this publication is the sole responsibility of the Consortium partners listed herein and does not necessarily represent the view of the European Commission or its services.

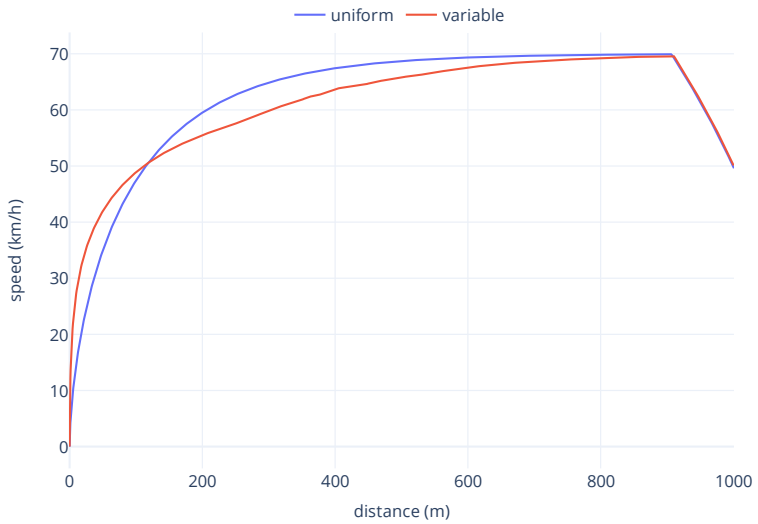

Figure 30: Speed as a function of distance for an example link, illustrating the profiles generated via a Gipps' model with a^{max} either uniform or variable.

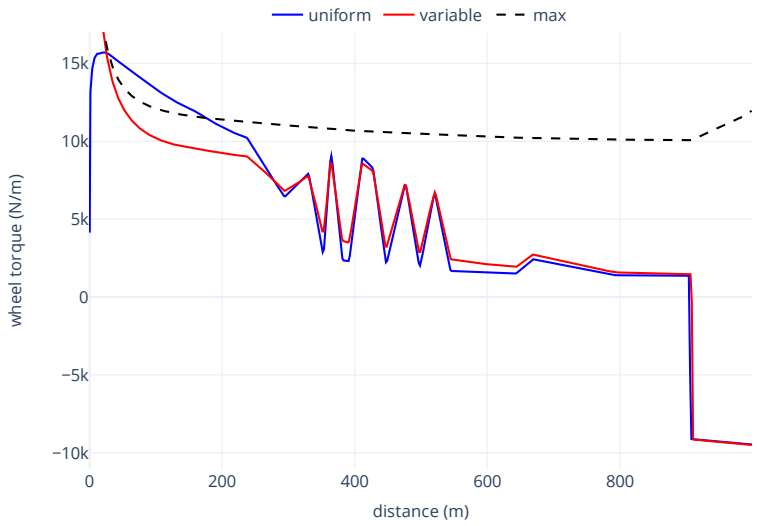

Figure 31: Wheel torque as a function of distance for an example link, illustrating the different profiles generated via a Gipps' model with a^{max} either uniform or variable, compared to the maximum wheel torque physically realizable by the HDV.

3.3.3 Energy Consumption Calculation

Once the speed profile and acceleration constraints are established, we compute the power required at the wheels:

$$P_{wheel} = T_{wheel} \cdot \frac{v}{r}. \tag{27}$$

The actual power consumed by the motor is then derived by incorporating the overall efficiency η (gearbox, battery and motor efficiencies) and the regenerative breaking ratio R_{regen}.

$$P_{motor} = \begin{cases} \frac{P_{wheel}}{\eta}, & P_{wheel} \geq 0 \\ P_{wheel} \cdot \eta \cdot R_{regen}, & P_{wheel} < 0 \end{cases} \tag{28}$$

This project has received funding from the European Union's HORIZON EUROPE research and innovation programme under grant agreement No. 101096028. The content of this publication is the sole responsibility of the Consortium partners listed herein and does not necessarily represent the view of the European Commission or its services.

The power consumed by the motor for the example link previously discussed is illustrated in Fig. 4. It can be observed that in absence of a dynamic definition of a^{max}, the motor power is largely overestimated, leading to poor accuracy in the prediction of the energy consumption.

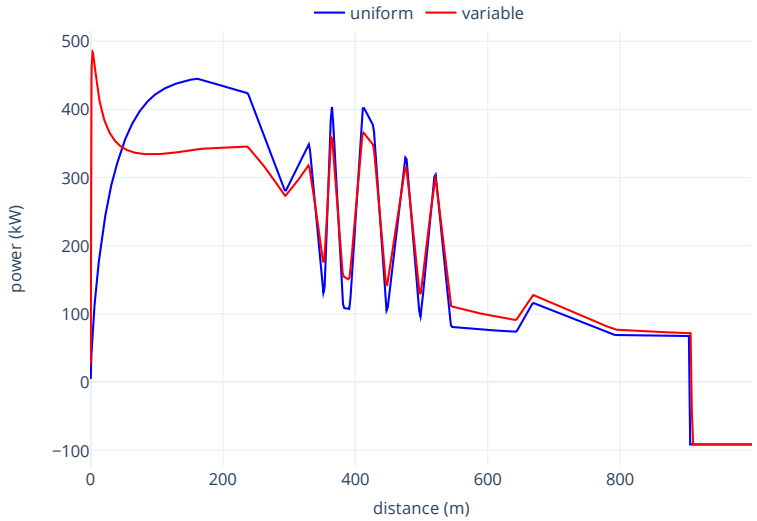

Figure 32: Motor consumption as a function of distance for an example link, illustrating the different profiles generated via a Gipps' model with a^{max} either uniform or variable.

3.3.4 Battery State-of-Charge (SOC) Evolution

To track battery usage, we model the evolution of SOC using the following equation:

$$C\,\frac{dq}{dt} = -P_{bat}(q,P) \tag{29}$$

where q is the SOC, C is the battery capacity, and $P = P_{motor} + P_{aux}$ with P_{aux} represents auxiliary power consumption. The battery power P_{bat} is computed as:

$$P_{bat}(q,P) = \begin{cases} \min\left(P_{bat}^{max}\ , \frac{P}{\eta_{bat}}\right)\ , & if\ P > 0 \\ \max\left(P_{bat}^{min}, \eta_{bat}\cdot P\right), & if\ P < 0 \end{cases} \tag{30}$$

Finally, the total energy consumed over a travel time T is given by:

$$E = \int_0^T \frac{P_{bat}(q(\tau))}{C}\,d\tau\,. \tag{31}$$

This allows us to quantify battery depletion for each driving segment accurately.

During charging, the charging time T_C required to reach a final SOC level q_2 from an initial level q_1 can be obtained by inverting the SOC dynamics:

$$T_C = \int_0^{T_C} C\,\frac{dq(\tau)}{P_{bat}(q(\tau),P_C)}\,d\tau = \int_{q_1}^{q_2} \frac{C}{P_{bat}(q,P_C)}\,dq\,, \tag{32}$$

where P_C is the rated charging power of the charging station. In practice, the calculation of this integral is replaced by empirical charging curves for the IVECO BEV, that relate SOC to charging time for various charger power levels, see Figure 33.

This project has received funding from the European Union's HORIZON EUROPE research and innovation programme under grant agreement No. 101096028. The content of this publication is the sole responsibility of the Consortium partners listed herein and does not necessarily represent the view of the European Commission or its services.

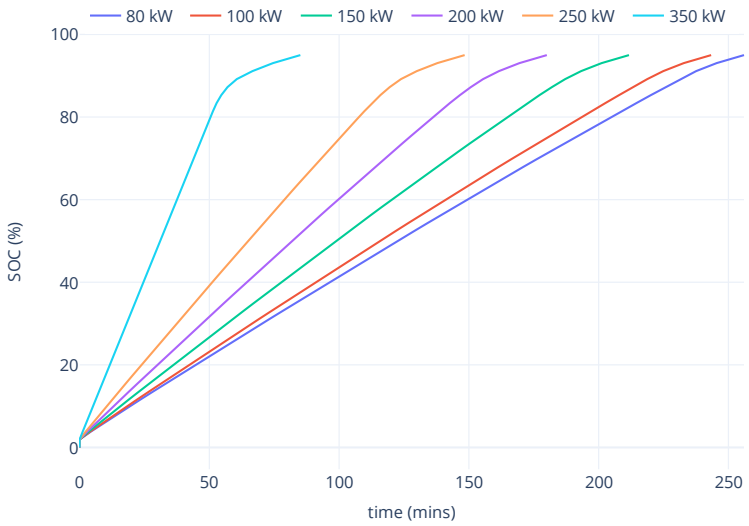

Figure 33: Charging curves for the 350kWh battery pack of the IVECO BEV under study, as a function of the SOC and the power of the charger to which the vehicle is connected.

3.4 Charging Network Model

To represent the charging network, we assume that a comprehensive global database providing detailed information about charging infrastructure is available. This must include data on charging stations within the geographical area of interest: location (latitude and longitude), charging capabilities, i.e., available charging power (e.g., 22 kW, 50 kW, etc.), supported connector types, number of charging points; status information, i.e., availability and operational status, prices per kWh.

For our purpose, we retain only those charging stations that are sufficiently close to the itineraries generated for the specific origin/destination pair under consideration, ensuring that the detour required to access a station is minimal and practical. The proximity-filtered charging station data is then incorporated into the graph structure representing the itineraries. This process involves :

- mapping charging points to the graph, i.e. for each charging station near an itinerary, the closest node in the original graph is identified based on geographical proximity. The identified node is labeled as a *charging node*.
- adding attributes to charging nodes such as, the name of the operator managing the station, the charging power available and the distance from the station to the actual node coordinates (detour distance).

To improve the accuracy of charging station identification, it is further convenient to introduce an {ad hoc} segmentation strategy. Specifically, road links longer than a given threshold, e.g. 5 km, could be divided into smaller segments to provide a more detailed representation of the road and facilitate the identification of charging stations. This is particularly important because charging stations are

identified based on their proximity to route waypoints, rather than actual links. As a result, long road links can lead to distant nodes, potentially causing the omission of stations along the route. By segmenting these links, we ensure a finer-grained road network representation that enhances station identification while preserving the essential characteristics of the original route.

3.5 Eco-charging

The eco-charging problem consists in determining an optimal *trip plan* for a vehicle traveling from an origin $x_0 = (lat_0, lon_0)$ to a destination $x_0 = (lat_\star, lon_\star)$, given an initial battery SOC q_0. The concept of eco-charging is an extension of the concept of eco-routing, in the same measure that a trip plan for a specific

This project has received funding from the European Union's HORIZON EUROPE research and innovation programme under grant agreement No. 101096028. The content of this publication is the sole responsibility of the Consortium partners listed herein and does not necessarily represent the view of the European Commission or its services.

origin/destination pair is an extension of the concept of itinerary. An itinerary is in fact primarily focused on routing, i.e., the selection of the sequence of road links the vehicle must follow to travel from the origin to the destination. A trip plan, on the other hand, is a more comprehensive concept that extends the idea of an itinerary by incorporating both driving and charging decisions, i.e., the drive-style that must be adopted, where the user should stop for charging and the quantity charged.

e-LDV algorithms focus on minimizing trip time through advanced computational methods like shortest-path algorithms and Mixed Integer Linear Programming (MILP), see for example [20-22]. These approaches leverage existing charging infrastructure, incorporating variables like battery range, charging station locations, traffic conditions, and speed adjustments. The flexibility of light-duty EVs allows for dynamic route optimization, addressing range anxiety through real-time charging decisions and balancing the fastest and most economical routes. Heavy-duty electric trucks, however, face more intricate challenges due to significant payload affecting energy consumption and driving dynamics, increased sensitivity of energy expenditure to road slope and curvature, as well as wind forces, limited onboard energy, and the demands of long-haul operations. Algorithms for these vehicles employ diverse techniques to address complex constraints, see for example [23, 24]}. These studies highlight critical distinctions between routing strategies for e-LDVs and e-HDVS. Heavy-duty electric trucks require significantly higher charging power, more frequent charging stations, and strategic infrastructure development compared to light-duty EVs. Range anxiety is a major constraint for heavy-duty vehicles due to the high stakes of long-haul operations, with limited route flexibility exacerbating the issue. Charging time optimization is also more critical for heavy-duty trucks, as delays impact operational schedules [25].

In the following subsections, we formulate the traditional routing problem, setting the basis for incorporating first driving, then charging decisions.

3.5.1 Routing problem

To describe the routing problem, we rely on the structured representation of the road network combined with the e-HDV model, both provided in Section 3.2. Let us define then the topological structure of the road network as a directed connected graph $G(X, E)$, characterized by a set $X$of nodes representing geographical locations associated to intersections or waypoints and E represents a set of edges associated to directed road links between these nodes. Any pair of nodes admits at most one (directed) edge. A solution, or *itinerary*, for G can be then characterized either by a sequence of connected nodes $X_\star = \{x_0, \dots, x_\star\} \subset X$ or, equivalently, a sequence of adjacent edges $E_\star = \{(0, j), \dots, (k, \star)\}$.

As already discussed, the vehicle's motion is constrained by several factors. A first set of constraints is dictated by the road network characteristics, such as the physical properties of the road links. Each road link $(j, k) \in E$ is associated with attributes such as length L_{jk} and legal speed limit V_{jk}. Traveling along links might be subject to tolls. Hence, each edge $(j, k) \in E$ further associates an economic cost attribute C_{jk}. Each node $j \in X$ is characterized by an end speed attribute V_j, denoting the maximum speed to be guaranteed when arriving at such node. Speed limits influence the *legally* realizable speed profile along each road link. A second set of constraints is associated with the vehicle's powertrain dynamics, as these are governed by constraints on acceleration, braking, and power usage. These constraints are dictated by the vehicle's motor, regenerative braking efficiency, and battery characteristics. They determine, together with the road network physical characteristics, the *physically* realizable speed profile $v_{jk}$for each road link, by imposing limits on acceleration, deceleration, and energy recuperation along the journey. Consequently, largely influencing two additional attributes that are associated to each road link: travel time $T_{jk}$and energy consumption E_{jk} . Based on this description, the traditional routing problem can be thus formulated as the problem of determining an *itinerary* $E_\star \subset E$ that minimizes a weighted combination of the overall energy consumption, travel time and economic cost:

This project has received funding from the European Union's HORIZON EUROPE research and innovation programme under grant agreement No. 101096028. The content of this publication is the sole responsibility of the Consortium partners listed herein and does not necessarily represent the view of the European Commission or its services.

$$J = \sum_{(j,k)\in E_\star} J_{jk}, \tag{33}$$

with $J_{jk}(E_{jk}, T_{jk}, C_{jk}) = \gamma_E E_{jk} + \gamma_T T_{jk} + \gamma_C C_{jk}$, where positive scalars γ_E, γ_T and γ_C are user-defined weightings that reflect the relative importance of energy consumption, travel time, and economic costs and J_{jk} denotes the per-edge driving cost. The routing problem can be the solved by applying shortest path algorithms, e.g. Bellman-Ford, to the graph.

3.5.2 Smart driving

Traditional routing problems are typically focused on the selection of the optimal route based solely on geographic factors like distance and road characteristics. The routing decisions usually assume a constant, predetermined driving style, without considering the driver's actual behavior, disregarding the significant impact that this may have both travel time and energy consumption, thereby influencing the overall cost $J$of the trip.

This behavioral flexibility can be introduced by allowing the selection of different reference speeds V^{ref} in the Gipps car-following presented in Section 3.3, enabling the optimization process to adapt the trip plan to specific user preferences. Incorporating driving style into the routing process requires an extension of the traditional routing graph$G$. In the original graph in fact, any two nodes $j, k \in X$ are connected by a single directed edge$(j, k) \in E$, representing a specific path between them. This edge corresponds to a single, predefined speed profile, which dictates a fixed travel time and energy consumption. However, different driving strategies can affect both these factors. For example, an *aggressive driver* might take sharper accelerations, use more power for higher speeds, and thus consume more energy and time. On the other hand, a *cautious driver* would adopt a more conservative speed profile, reducing energy consumption but possibly increasing travel time. To model this variation, we construct a multi-graph $G_D(X, E_D)$, where E_D denotes the extended set of edges, consisting *multiple directed edges* between each pair of connected nodes, where each edge corresponds to a different *driving strategy* adopted. Based on this description, the eco-routing problem with driving decisions can be thus formulated, similarly to the previously defined routing problem, as the problem of determining a solution $E_\star \subset E_D$ that minimizes a weighted combination of the overall energy consumption, travel time and economic cost, using the same per-edge cost function J_{jk} used in the eco-routing problem, but now applied to any$(j, k) \in E_D$. The routing problem with driving decisions can be solved, similar to the traditional routing problem, by applying Bellman-Ford algorithm to the graph.

3.5.3 Algorithm design

The traditional routing framework, like eco-driving, can be extended to incorporate charging decisions by augmenting the graph $G_D(X, E_D)$ with self-loop edges at nodes corresponding to charging stations. These self-loop edges would represent charging events where the vehicle replenishes its SOC at specific nodes $i \in S$ along its route. This extension allows for the inclusion of charging stops, where cycling over a node signifies a charging process, enabling the SOC to increase according to charging decisions. However, this extension alone does not fully resolve the critical challenge of managing the SOC constraints throughout the journey. A direct approach to ensuring feasibility is to employ a constrained shortest path (CSP) algorithm, which finds an optimal route while enforcing SOC constraints. However, the CSP problem with SOC constraints is NP-hard in general, meaning that finding the optimal solution is computationally intractable for large networks.

To cope with this problem, we propose to construct a state-augmented graph $G_C(X_C, E_C)$ that extends the traditional concept of routing graph by incorporating the vehicle's SOC $q$as a node attribute, in addition to its geographic position$x$. This approach enables a unified representation of both routing and energy dynamics, ensuring that the feasibility constraints related to battery depletion are naturally integrated into the graph structure.

This project has received funding from the European Union's HORIZON EUROPE research and innovation programme under grant agreement No. 101096028. The content of this publication is the sole responsibility of the Consortium partners listed herein and does not necessarily represent the view of the European Commission or its services.

A node j of the state-augmented graph is characterized by the pair(x_j, q_j), where $x_j$represents the vehicle's geographic location and q_j represents its battery SOC at that location. An edge $(j,k) \in E_D$ of the state-augmented graph can be either a *driving edge* or a *charging edge*.

A *driving edge* between node j and node k represents vehicle motion on a road link between location x_j to location x_k, with$x_j \neq x_k$, resulting in different SOC levels upon arrival atx_k, depending on the driving strategy adopted. For instance, an aggressive driving strategy may lead to a lower SOC, while an energy-efficient strategy may preserve more charge. As for the routing problem, the cost-function J_{jk} can be used to determine the cost of each driving edge, where scalars $\gamma_E, \gamma_T, \gamma_C$ are positive scalars selected according to user's preferences.

A *charging edge* between node j and node k represents a charging decision operated while the vehicle is at rest at a charging station, i.e.$x_j = x_k \in S$. The actual charging is captured by the SOC increase from $q_j$to q_k, with $q_k > q_j$. By means of these edges, paths for progressively increasing the SOC can be added to the graph, modeling appropriately the effect of charging stops as a function of the duration of the stop, the power rating of the charger used and the economic cost for charging. Note that in contrast with the cost J_{jk} associated with driving edges, which may depend on energy consumption, travel time, and economic (tolls) cost, the cost associated with charging edges can be a weighted combination of charging time and the economic (charging) cost only, i.e., it is independent from the (negative) energy consumption induced by the charging process. The per-edge cost associated to a charging edge is then given by:

$$J_{C,jk} = \alpha_T T_{jk} + \alpha_C C_{jk}, \tag{34}$$

where α_T, α_C are user-defined weightings that reflect the relative importance of charging time and economic costs, while $J_{C,jk}$ denotes the per-edge charging cost. This is consistent with the fact that energy stored in the battery during charging does not add to the overall energy consumption of the trip, but it simply replenishes the battery for further use. The construction of the state-augmented graph can be performed iteratively via the algorithm described in Table 9.The input taken by the algorithm consists of the graph $G_D(X, E_D)$, capacity C and limits of the battery $[q_{min}, q_{max}]$ and a scalar Δq denoting the charge unitary step allowed during recharge. The output consists in the state-augmented graph $G_C(X_C, E_C)$. In line with what discussed in the previous sections, a Bellman-Ford algorithm can be used to determine the optimal trip plan.

Table 9: Eco-charging algorithm pseudocode.

- Initialize graph $G_C$with initial node (x_0, q_0)
- for each node $(x_j, q_j) \in G_C$
  - for $x_k \in$ succ(x_j)
    - Obtain driving edge attributes E_{jk}, T_{jk}, C_{jk}
    - Compute driving cost $J_{jk}(E_{jk}, T_{jk}, C_{jk})$
    - Compute next SOC $q_k = q_j - E_{jk}/C$
    - if $q_k \in [q_{min}, q_{max}]$
      - Add edge $(x_j, q_j) \rightarrow (x_k, q_k)$ with cost J_{jk} to G_C
      - if $x_k \in S$
        - Round up q_k to $\bar{q}_k$ (nearest SOC)
        - Compute charging cost $J_{C,jk}$
        - Add charging edge (x_k,q_k) → (x_k,q_k) to G_C
        - while $q_k + \Delta q \leq q^{max}$
          - Compute cost $J_{jk}(0, \gamma_2, \gamma_3)$
          - Add edge (x_k,q_k) → (x_k,$q_k + \Delta q$) to G_C
          - $q_k = q_k + \Delta q$

This project has received funding from the European Union's HORIZON EUROPE research and innovation programme under grant agreement No. 101096028. The content of this publication is the sole responsibility of the Consortium partners listed herein and does not necessarily represent the view of the European Commission or its services.

3.6 Eco-driving

Eco-driving strategies are aimed at minimizing fuel consumption and promoting sustainable driving practices in heavy-duty vehicles. It involves adopting a range of driving techniques and strategies that optimize energy efficiency while ensuring safety and comfort for both drivers and passengers. By providing drivers with recommended speed profiles and real-time guidance, the eco-driving strategy empowers them to make fuel-efficient choices and reduce their carbon footprint. In the context of the project, the eco-driving strategy is one of the connected functions developed. Its objective is to showcase the potential of connectivity in reducing energy consumption in real driving conditions, contributing to the global EMPOWER objectives. The work carried out in the LONGRUN project, which also aimed to develop an eco-driving strategy for conventional ICE HDVs, serves as a valuable source of inspiration and provides transferable solutions for the current approach [16, 26].

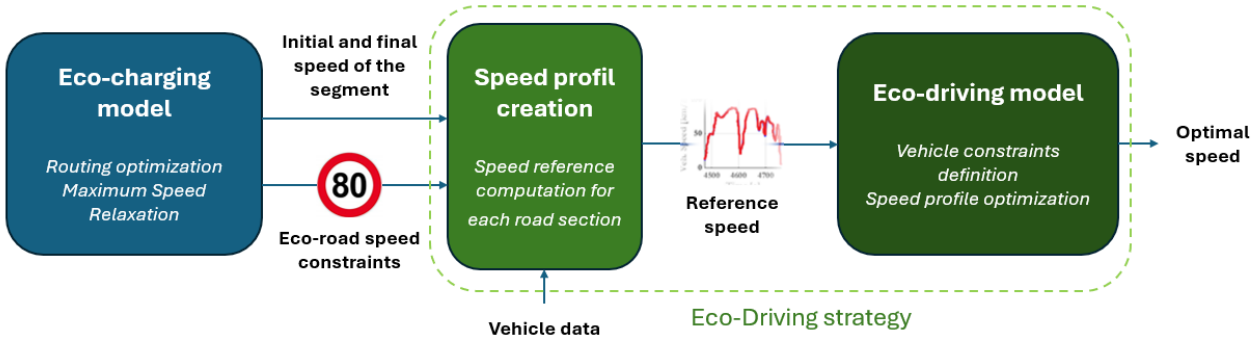

Figure 34: Workflow for eco-driving strategy

The eco-driving strategy developed in this project operates in an offline mode. Rather than delivering real-time recommendations during the journey, it generates an optimal speed profile beforehand, relying on models of both the route and the vehicle—for more details refer to Section 3.2 and Section 3.3. This approach allows for the analysis and optimization of energy consumption in realistic driving conditions, while ensuring that the computed strategy remains feasible and safe.

The starting point of the eco-driving strategy consists in retrieving detailed route information provided by the outputs of the eco-charging algorithm. This includes data such as the maximum speed for each road segment, the initial and final speeds, as well as potential complete stops (e.g., traffic lights, stop signs, or vehicle recharging events). Based on this information, an intermediary speed profile is generated using the driver model discussed in Section 3.3. This profile respects all speed and infrastructure constraints and serves both as a baseline for optimization and a reference for comparing fuel consumption performance.

To minimize fuel consumption effectively, the eco-driving algorithm requires a model that is both accurate and computationally efficient. An analytical model serves this purpose by providing a simplified yet sufficiently accurate mathematical representation of the vehicle's dynamics. Unlike detailed consumption maps, which are data-heavy and not well-suited for fast, real-time optimization, the analytical model allows the formulation of a solvable optimization problem. It captures the essential relationships between control inputs (like wheel and braking torque) and vehicle behavior (position, speed, and fuel use) through differential equations, making it possible to derive optimal control strategies with significantly lower computational cost.

The methodology for generating the optimized eco-driving profile is organized into four key steps:

1. Feasibility adjustments: The intermediary input speed profile is generated segment by segment to ensure physical and operational feasibility, considering the analytical vehicle model and road infrastructure via the procedure described in Section 3.3.

This project has received funding from the European Union's HORIZON EUROPE research and innovation programme under grant agreement No. 101096028. The content of this publication is the sole responsibility of the Consortium partners listed herein and does not necessarily represent the view of the European Commission or its services.

2. Data extraction: From the adjusted profiles, key parameters such as segment length, travel time, and initial/final speeds are extracted. This data is used to set up the optimization problem for each segment.
3. Segment-level optimization: An optimization problem is formulated for each segment, with the objective of minimizing a cost function that captures fuel consumption and driver control effort. The optimization respects legal speed limits and additional route constraints.
4. Profile synthesis: Once all segments are individually optimized, the resulting speed profiles are merged to form a continuous eco-driving speed profile for the full route. This profile represents the final output of the strategy.

To streamline the optimization process very short segments (less than 100 meters or 10 seconds in duration) are removed, as they provide too few data points for effective optimization. By focusing on segments with high optimization potential and leveraging both vehicle modeling and detailed route information, this offline eco-driving strategy contributes to achieving the overall goals of the project: reducing fuel consumption and emissions through intelligent, connected driving technologies.

3.6.1 Theoretical Framework and Optimization Methodology

The goal of this work is to optimize the velocity trajectory and control commands (traction and braking torque) of a vehicle to minimize its energy consumption along a known trajectory, while respecting dynamic and environmental constraints. This optimization is formulated as an optimal control problem and solved using the Radau collocation method, relying on the CasADi library and the IPOPT solver.

3.6.2 Formulation of the Optimal Control Problem (OCP)

The vehicle's dynamic system over a segment of length ℓ, characterized by a maximum legal speed $\bar{V}$ is modeled by continuous dynamic equations, which in state-space form reads:

$$\dot{x}(t) = f\big(x(t), u(t)\big), \quad x(0) = x_0 \tag{35}$$

where:

- $x(t) = [x_1(t)\ x_2(t)\ x_3(t)] \in \mathbb{R}^3$ is the state vector containing:
  - $x_1(t) = s(t)/\ell$: normalized relative position,
  - $x_2(t) = v(t)/\bar{V}$: normalized speed,
  - $x_3(t) = c(t)$: cumulative consumption.
- $u(t) \in \mathbb{R}^2$ is the control vector with:
  - $u_1(t) = T_{wheel,drive}/\ T^{max}_{wheel}(v)$: normalized traction control (motor torque, [0,1]),
  - $u_2(t) = \ T_{wheel,brake}/\ T^{max}_{wheel}(v)$: normalized braking control (brake torque, [-1,0]).

The optimization objective is to minimize the cumulative consumption at the final time t_f :

$$\min_{x,u} J = c(t_f) \tag{36}$$

subject to the following constraints:

- **Vehicle dynamics**:

$$\dot{x}(t) = f\big(x(t), u(t)\big) \tag{37}$$

This project has received funding from the European Union's HORIZON EUROPE research and innovation programme under grant agreement No. 101096028. The content of this publication is the sole responsibility of the Consortium partners listed herein and does not necessarily represent the view of the European Commission or its services.

- **Initial and final conditions on position and speed**:

$$x(0) = x_0,\ x(t_f) = \ell \tag{38}$$

- **Control constraints**:

$$u(t) \in U = \{u \in \mathbb{R}^2 : u_1 \in [0,1],\ u_2 \in [-1,0],\ u_1 \cdot u_2 = 0\} \tag{39}$$

- **Physical constraints on motor torque and braking torque**:

$$T_{wheel,drive}(t) \le T_{wheel}^{max}(v),\ T_{wheel,brake}(t) \ge T_{wheel}^{min}(v) \tag{40}$$

where these torques are functions of speed and are extracted from analytical or empirical models.

3.6.3 Discretization by Collocation

The collocation method transforms the continuous problem into a discretized nonlinear optimization problem (NLP). The time domain $[0, t_f]$ is divided into N intervals of length $h = t_f/N$.

Each interval is discretized using Radau collocation points, allowing a local polynomial approximation of the state trajectory:

$$x_k(\tau) \approx \sum_{j=0}^{d} L_j(\tau) x_{k,j} \tag{41}$$

where $L_j(\tau)$ are Lagrange polynomials defined at the collocation points $\tau_j \in [0,1]$.

The dynamic equations are enforced at the collocation points:

$$\sum_{j=0}^{d} C_{j,r} x_{k,j} = h \cdot f(x_{k,r}, u_k),\ r = 1, \dots, d \tag{42}$$

where:

- $C_{j,r}$ are the derivative coefficients of the Lagrange polynomials,
- h is the interval size,
- $f(x_{k,r}, u_k)$ is computed using the vehicle's dynamic model

The continuity of the solution between intervals is ensured by a constraint:

$$x_{k+1,0} = \sum_{j=0}^{d} D_j x_{k,j}, \tag{43}$$

where D_j are the evaluation coefficients at $\tau = 1$ for the interpolation polynomials.

3.6.4 Numerical Solution with IPOPT

All problem variables (states and controls) are gathered into a single variable z. The problem is then transformed into an NLP of the form:

$$\min_z c(z) \quad s.t.\ \ g(z) = 0,\ \ z_{min} \le \mathrm{z} \le \mathrm{z}_{\max}, \tag{44}$$

where:

- $c(z) = x_{N,0}[2]$represents the final consumption,
- $g(z)$ includes the dynamic, continuity, boundary, and constraint conditions.

This project has received funding from the European Union's HORIZON EUROPE research and innovation programme under grant agreement No. 101096028. The content of this publication is the sole responsibility of the Consortium partners listed herein and does not necessarily represent the view of the European Commission or its services.

The solution algorithm uses IPOPT, a solver based on an interior-point method, which is particularly suited for large-scale, nonlinear problems like the one at hand.

3.6.5 Optimization-friendly consumption model

As previously discussed, the key variable to be optimized using the collocation method is the vehicle's energy consumption. To achieve this, it is essential to rely on a representative and sufficiently accurate consumption model. As described in Section 3, this function consists of two distinct parts: the positive power traction phase, and the negative power braking phase, where in the latter a scaling factor is introduced to account for regenerative braking, recognizing that not all braking energy can be recuperated due to longitudinal stability. Recall the motor power is then given by

$$P_{motor} = \begin{cases} \frac{P_{wheel}}{\eta}, & P_{wheel} \geq 0 \\ P_{wheel} \cdot \eta \cdot R_{regen}, & P_{wheel} < 0 \end{cases} \tag{45}$$

which is a continuous function non differentiable in zero—that is, at the transition point between traction and braking. This lack of differentiability presents a challenge for the optimization algorithm, which relies on collocation methods and symbolic processing of mathematical expressions. Such approaches require indeed the use of analytical functions that are differentiable across the entire domain. As a result, the original consumption model must be reformulated to meet these mathematical constraints.

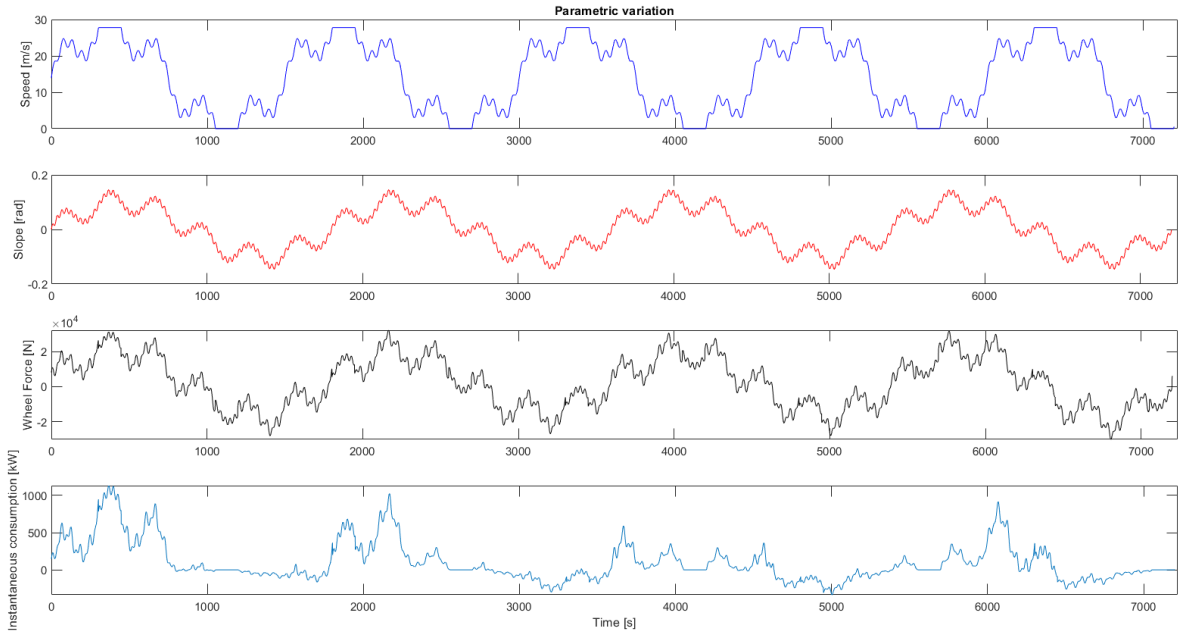

Figure 35: Parametric variation

To overcome this limitation, an approximation of the energy consumption is constructed using polynomial regression. This approximation is based on two key parameters: the vehicle's speed and the force applied to the wheels. To ensure complete and uniform coverage of the domain, a synthetic dataset is generated from a fictitious route that smoothly spans the full range of relevant values. Specifically, speed is varied from 0 to 100 km/h, and the road slope is varied between +0.15 and –0.15 radians. For each combination of speed and slope, the corresponding wheel force is recalculated, and the associated energy consumption is evaluated. A 10th-degree polynomial regression is then applied to this dataset. The high degree of the polynomial allows for precise modeling of the nonlinear variations in consumption across the domain, while ensuring that the resulting function remains continuous and differentiable.

This project has received funding from the European Union's HORIZON EUROPE research and innovation programme under grant agreement No. 101096028. The content of this publication is the sole responsibility of the Consortium partners listed herein and does not necessarily represent the view of the European Commission or its services.

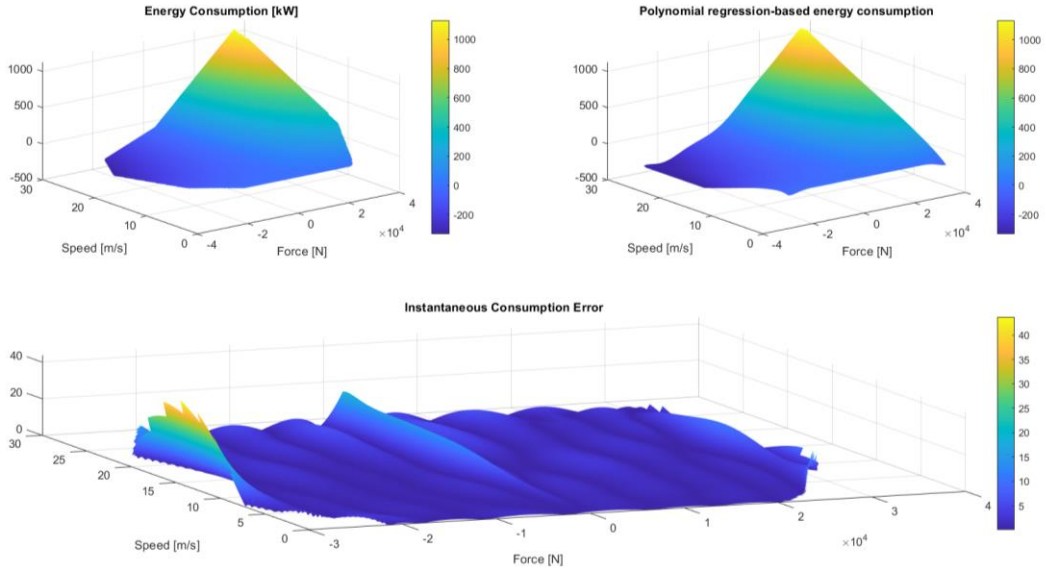

Figure 36: Polynomial regression-based energy consumption

The outcome of this process is an analytical, fully differentiable function expressed in terms of vehicle speed and wheel force. This function can be directly integrated into the optimization algorithm, enabling precise and smooth evaluation of energy consumption at every step of the simulation. Although this approximation may introduce slight deviations from the original model, it ensures mathematical compatibility with the solver requirements while maintaining excellent overall accuracy.

3.7 Results

To validate the algorithm, we first define the origin/destination pair. The origin is set at Gruber Logistic headquarters, near Verona, Italy, while the destination is set at IVECO headquarters in Ulm, Germany. This origin-destination pair aligns with one of the test routes identified by the EMPOWER project, enabling us to assess the algorithm's performance on a highway corridor frequently traveled by HDVs.

3.7.1 Eco-charging

As already explained in Section 3.2, we rely on a GIS to extract detailed road network characteristics, including road geometry, segment lengths, legal speed limits, and real-time traffic conditions. Specifically, we use HERE webservice, which offers comprehensive road attributes, such as lane structures, connectivity, and speed regulations, along with live and historical traffic data. Additionally, it processes as input basic vehicle information, such as height, overall weight, and the potential for carrying hazardous goods, to ensure that the proposed itinerary complies with road network restrictions that apply to the specific vehicle's profile. This ensures that the suggested routes are appropriate for the vehicle's characteristics and adhere to all relevant regulations and safety standards.

For the modeling of the charging network infrastructure, we rely instead on OpenChargeMap. It is an open-source platform designed to provide detailed and accurate information about electric vehicle charging stations worldwide. It aggregates data from a variety of sources, including public, private, and commercial charging networks, offering a comprehensive database of charging stations. The platform enables users to access key information about each charging point, including its location, charging capabilities, and current availability.

For the specific origin/destination pair under study, we limit the alternative itineraries generated by HERE to two (see Figure 37). To maintain route relevance, we limit our search via OpenChargeMap to stations situated within 1 km of the proposed itineraries. When multiple charging points are available at a station, we prioritize the one with the largest power rating, as it would generally provide the fastest charging, reducing downtime

This project has received funding from the European Union's HORIZON EUROPE research and innovation programme under grant agreement No. 101096028. The content of this publication is the sole responsibility of the Consortium partners listed herein and does not necessarily represent the view of the European Commission or its services.

and improving overall trip efficiency. To comply with e-HDV requirements, as well as to guarantee that only reasonably fast chargers are adopted, we consider only chargers with power greater than 80 kWh.

Next, driving strategies are incorporated into the graph, following the approach described in Section, resulting into a multi-graph $G_D(X, E_D)$. The current settings allow users significant flexibility in adopting different driving practices, which can enhance adaptability but also introduce challenges. In terms of driving practices, let us assume that three different strategies (aggressive, cautious, average) can be adopted by the user. This flexibility, is only applicable to non-urban road links $(j,k) \in E$, where the legal speed limit $\bar{V}_{jk} \geq 0$ km/h. Driving behavior along edges connecting the same nodes differs in terms of the reference speed $\bar{V}_{jk}^{ref} \geq 0$ assigned via the Gipps' car-following model, thus resulting in different energy consumption and travel time along the link. For the aggressive behavior we assign $\bar{V}_{jk}^{ref} = \bar{V}_{jk}$, for the average $\bar{V}_{jk}^{ref} = 0.9 \cdot \bar{V}_{jk}$, and for the cautious $\bar{V}_{jk}^{ref} = 0.9 \cdot \bar{V}_{jk}$. An example of the speed profiles generated for a link of 5 km, corresponding to different driving styles, is illustrated in Figure 38.

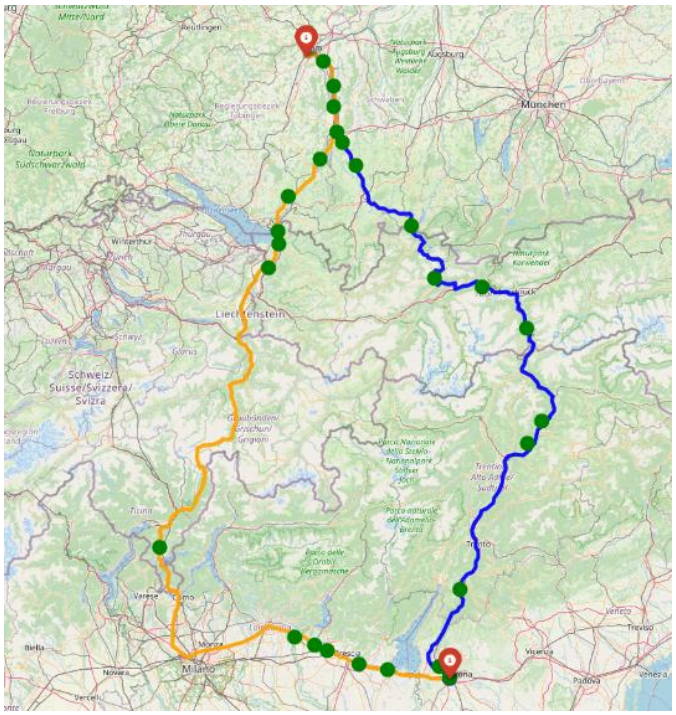

Figure 37: Graph generated from the routes and charging point locations obtained using HERE and OpenChargeMap webservices, for the origin/destination pair under study.

Now, a key consideration is that the large number of small road links may lead to a significant computational burden. Additionally, while users can switch between different driving styles, it is not realistic to expect frequent changes, especially on short consecutive links, as this could become overwhelming for the user. Another important observation is that allowing excessive flexibility in driving strategies may result in multiple possible driving sequences across a series of links, yet most of these combinations ultimately lead to similar total costs. As a result, this added flexibility does not substantially improve the optimization process.

This project has received funding from the European Union's HORIZON EUROPE research and innovation programme under grant agreement No. 101096028. The content of this publication is the sole responsibility of the Consortium partners listed herein and does not necessarily represent the view of the European Commission or its services.

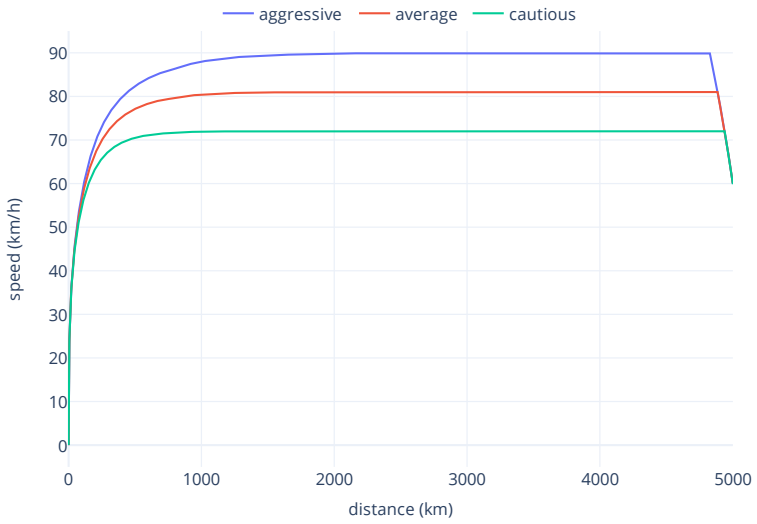

Figure 38: Speed profiles associated to different driving styles for a link $(j,k) \in E_D$ of length 5 km, zero initial speed, legal speed 90 km/h, end speed 60 km/h.

To address these challenges, we execute the algorithm for each of the itineraries suggested separately. Then, we proceed by aggregating links into macrolinks so to ensure that no road macrolink is shorter than 5 km, except for those directly connecting charging stations. This dimensionality reduction results in reduced graphs, one per itinerary, with fewer nodes and edges, significantly decreasing the computational burden while still retaining the essential characteristics of the routes. This aggregation not only simplifies the problem but also ensures that the macrolinks always have a positive cost, since the potential for negative energy consumption due to regenerative braking is averaged out over a macrolink. This approach prevents situations where the energy consumption could be negative, thus allowing to apply Dijkstra's algorithm efficiently, leading to faster computations.

To model the charging decision in conformity with the vehicle under study, we have to consider the vehicle's battery capacity $C = 350$ kWh. Moreover, we assume that charging decisions are made so that SOC can be charged only to levels that are multiple of a base SOC level, corresponding to 5% of the total capacity, i.e., $\Delta q = 0.05\ C$. For charging times as a function of the SOC and of the power charger employed are illustrated, we refer to Figure 33 in Section 3.2.

Next, it is possible to apply the eco-charging algorithm to the multi-graph $G_D(X, E_D)$ to obtain the state-augmented graph $G_C(X_C, E_C)$, which contains all feasible trip plans for reaching the destination from the origin, based on the alternatives provided by HERE webservice and the available charging stations provided by OpenChargeMap webservice. To illustrate flexibility of the proposed algorithm with respect to user preferences, we consider four different optimization criteria, which stem from different assignments of the per-edge cost function J_{jk}. The different options are illustrated in Table 10. They correspond to optimize total travel time (*fast*) travel time with the lowest charging economic cost (*fast-budget*), consumption with the fastest charging time (*eco-fast*), and consumption with the lowest charging cost (*eco-budget*).

Table 10: Assignment of the weights of the per-edge cost based on the optimization criteria adopted.

Mode	**Cost coefficients**	
fast	$\gamma_T = \alpha_T$	$\gamma_E = \gamma_C = \alpha_C = 0$
fast – budget	$\gamma_T = \alpha_C$	$\gamma_E = \gamma_T = \alpha_T = 0$
eco - fast	$\gamma_E = \alpha_T$	$\gamma_T = \gamma_C = \alpha_C = 0$
eco - budget	$\gamma_E = \alpha_C$	$\gamma_C = \gamma_T = \alpha_T = 0$

To assess performances of our solutions we further introduce a *baseline* solution. This assumes a fixed anxiety range for the user, which can be interpreted as the user knowing an estimate of the SOC consumption rate Δq

This project has received funding from the European Union's HORIZON EUROPE research and innovation programme under grant agreement No. 101096028. The content of this publication is the sole responsibility of the Consortium partners listed herein and does not necessarily represent the view of the European Commission or its services.

per kilometer. Thus, whenever the user approaches a charging station $i \in S$, he relies on measure of the current SOC q, and the estimated distance to the next station d, to determine whether a charging stop is necessary. Specifically, the user decides to stop if and only if $q < min(d\Delta q, 0.2)$, i.e., the decision to stop is driven by either the anxiety of not being able to reach the next charging point or by the SOC falling below 20%. If the user decides to stop, the amount of charge added is $min(q - d\Delta q + 0.1, q^{max})$. In other words, the SOC to be reached before leaving the station must be sufficient to guarantee that the vehicle can reach the next charging station, with an additional safety margin of 10%. In Table 11 we report the cumulated values of energy consumption E, travel time T and economic cost C, as well as the average speed v along the trip. In Table 12 we report the corresponding charging patterns, namely the cumulated values of energy charged E_C, charge time T_C and charging cost C_C, as well as the number of stops along the trip.

Table 11: Overall trip metrics for different optimization modes.

OVERALL TRIP				
Mode	E **(kWh)**	T **(min)**	C **(€)**	v **(km/h)**
baseline	627.9	764	278.2	71
fast	623.5	**637**	302.0	68.9
fast - budget	648.0	786	**244.3**	70
eco - fast	550.8	700	315.2	55.6
eco - budget	**550.5**	803	245.0	55.3

Table 12: Charging metrics for different optimization modes.

CHARGING PATTERNS				
Mode	E_C **(kWh)**	T_C **(min)**	C_C **(€)**	$stops$ **(#)**
baseline	378.5	328	158.2	4
fast	364.0	194	182.0	3
fast - budget	388.5	350	124.3	4
eco - fast	297.5	151	195.2	3
eco - budget	294.0	251	225.0	4

All solutions converge to the same route (highlighted in blue in Figure 37), covering a total distance of approximately 509 km and a toll cost of 120 €. As expected, solutions based on a more aggressive driving style—namely *baseline*, *fast*, *fast-budget* exhibit the highest energy consumption. These modes maintain an average speed of around 70 km/h and prioritize reduced travel time. Among them, the *fast* configuration achieves the shortest travel time of 637 min. In contrast, the *eco* modes, characterized by a more conservative driving style (average speed of approximately 55 km/h), achieve the lowest energy consumption, with both *eco-fast* and *eco-budget* consuming roughly 550 kWh. Despite similar energy profiles, these two configurations differ significantly in charging strategy and, consequently, in both charging time and economic cost. While *eco-fast* minimizes charging time (by nearly 100 minutes compared to *eco-budget*, it results in a higher overall cost—about 10 € more. Interestingly, the *fast-budget* solution demonstrates that substantial cost savings can be achieved without a major increase in total travel time compared to the baseline, though at the expense of elevated energy usage. Overall, these findings underscore the flexibility of the proposed optimization framework. By allowing users to prioritize different objectives—be it cost minimization, energy efficiency, or travel time reduction—the algorithm can be tailored to meet a broad range of user preferences and operational constraints. The different energy profiles are illustrated in Figure 39. It highlights how energy consumption varies along the route, with higher consumption occurring in sections requiring more power (e.g., steep inclines or high-speed driving). This provides further insight into how different solutions manage energy usage across the journey, reinforcing the idea that more efficient routes or driving styles contribute to lower overall energy consumption.

This project has received funding from the European Union's HORIZON EUROPE research and innovation programme under grant agreement No. 101096028. The content of this publication is the sole responsibility of the Consortium partners listed herein and does not necessarily represent the view of the European Commission or its services.

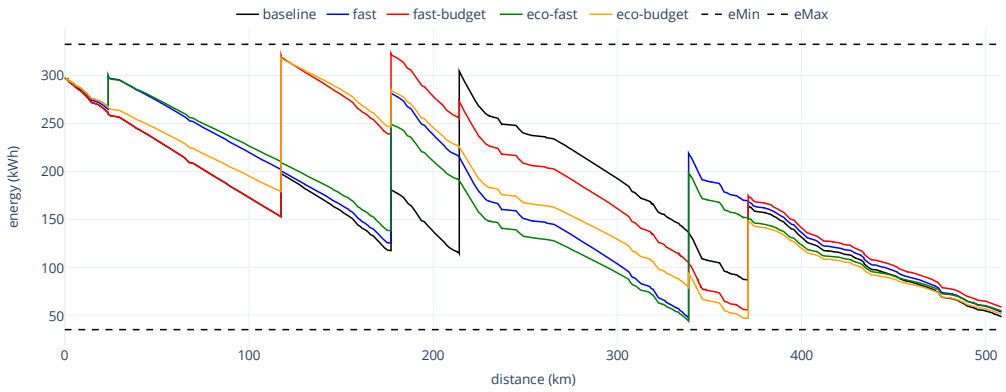

Figure 39: Energy consumption profiles resulting from different optimization criteria.

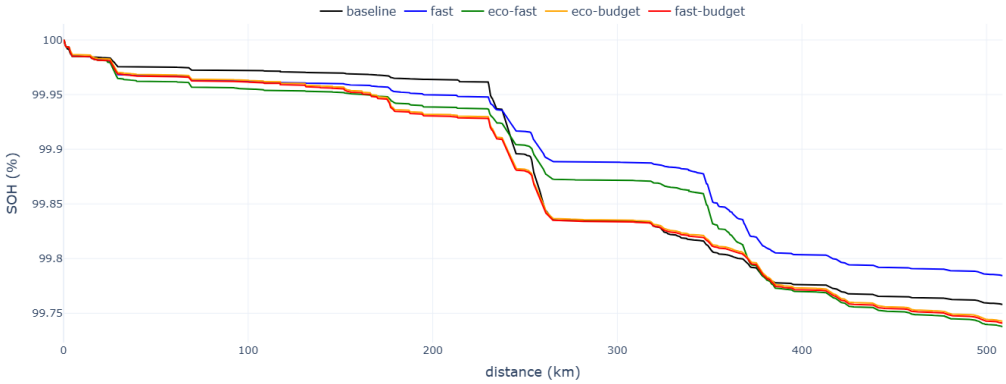

Figure 40: Evolution of the SOH compared to the evolution of the SOC for different optimization criteria that can be selected within the eco-charging strategy.

As a final contribution for the analysis of the eco-charging results we employ the ageing model described in Section 2.2 to evaluate the impact of the different solution on the battery SOH. Specifically, we employ Model 1 and Model 2 described therein to estimate battery degradation during driving and charging respectively. The results are illustrated in Figure 40. It is evident that the *fast* option results in the least degradation of the battery's SOH, followed by the *baseline* option. In contrast, the remaining options cause similar levels of battery degradation. Notably, degradation appears to be strongly influenced by the current SOC, both during driving and charging phases. Refer to Figure 39 for a detailed comparison.

3.7.2 Eco-driving

This section focuses on the validation of the eco-driving approach and presents a scenario based on the Verona-Ulm, including the more than 1000 intermediate waypoints—see Figure 37 (blue itinerary) for more details on this logged route. As already mentioned, this route has been carefully selected to represent a real-world driving scenario and will serve as a benchmark for evaluating connected strategies in the demonstration phase of the project.

To assess the validity of the consumption model used by the eco-driving strategy, which aims to minimize fuel consumption by providing the driver with an optimal reference speed to follow, the figure below compares the reference speed profile initially generated by the eco-driving algorithm based on the information provided by the eco-charging algorithm. The eco-driving algorithm operates by successively processing segments defined by the eco-charging module (the maximum, legal, initial, and final speeds for each segment). These segments are constructed based on each change in speed that may be imposed by the road along the route. For this section, the *ecofast* configuration has been selected as an example. It is important to note that, due to the nature of the eco-driving strategy—which involves more variations in the speed profile compared to the reference

This project has received funding from the European Union's HORIZON EUROPE research and innovation programme under grant agreement No. 101096028. The content of this publication is the sole responsibility of the Consortium partners listed herein and does not necessarily represent the view of the European Commission or its services.

strategy—we have chosen to present a detailed visualization of a specific segment of the speed profile and its corresponding consumption rate only.

The eco-driving algorithm leverages detailed route information to compute an optimal reference speed profile aimed at minimizing energy consumption. For each segment of the route, the algorithm first generates a feasible speed profile that accounts for the vehicle's dynamic constraints while ensuring compliance with legal speed limits. This preliminary profile serves as the initial guess for an optimization routine, which then determines the final output of the algorithm for each segment. For clarity, we refer to the initial input profile used in the optimization as the baseline reference speed profile, and to the resulting output profile as the optimal speed profile of the eco-driving algorithm.

Figure 41: Analysis of the entire route (altitude, speed, speed and consumptions as function of time)

The figure above illustrates the baseline and optimal reference profiles computed by the algorithm over the entire route, including key parameters such as speed, altitude, and energy consumption, together with the maximum and legal speed limits derived from the route and traffic constraints provided by the eco-charging outputs.

Figure 41 provides an overall representation of the eco-driving algorithm. From top to bottom, it shows the variation in altitude and road gradient, the vehicle's speed, the instantaneous fuel consumption, and the cumulative consumption. It is important to note that the selected route features significant changes in elevation, as the vehicle crosses the Alpine Mountain range.

The figure clearly displays the reference speed profile—referred to here as the Gipps profile—as well as the optimized speed profile, which is the output of the eco-driving algorithm. The instantaneous and cumulative energy consumption associated with this optimized speed profile are also shown. To explore the algorithm's behavior in more detail, several specific portions of the route have been selected for analysis, illustrating its response to different driving contexts. Some segments are representative of urban environments, characterized by frequent acceleration and braking phases, while others correspond to highway-like conditions, with long stretches of steady-speed driving.

This project has received funding from the European Union's HORIZON EUROPE research and innovation programme under grant agreement No. 101096028. The content of this publication is the sole responsibility of the Consortium partners listed herein and does not necessarily represent the view of the European Commission or its services.

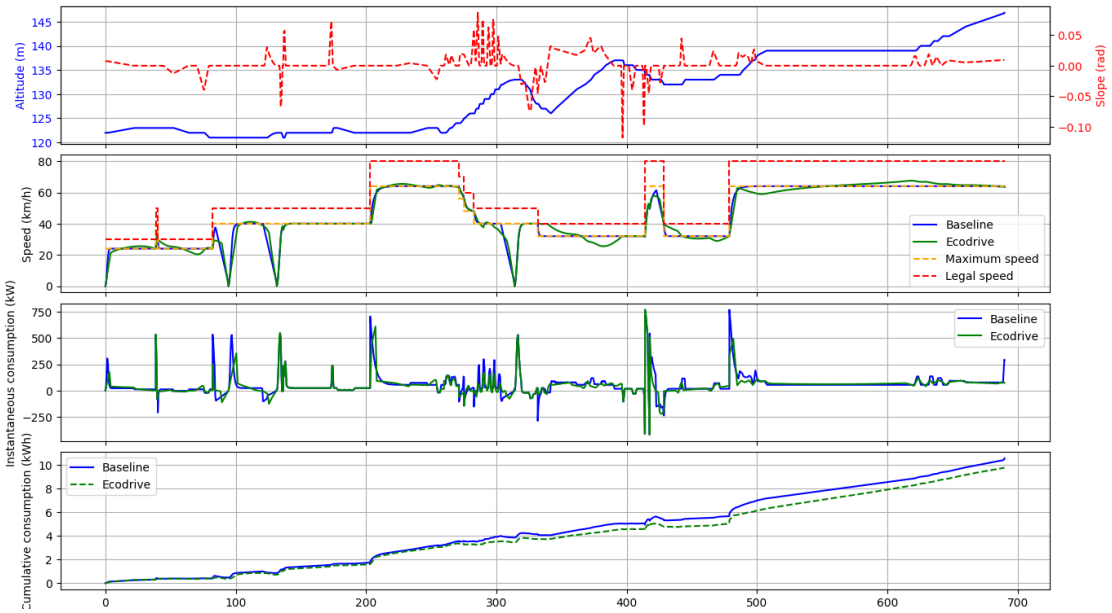

Figure 42: Analysis of urban segments (altitude, speed, speed and consumptions as function of time)

The urban-like segments of the route are marked by significant speed variations from one segment to the next. Numerous acceleration and deceleration phases can be observed, along with occasional full stops. This configuration offers the optimizer a high degree of flexibility in adjusting the vehicle's behavior.

In these conditions, since the legal speed limit is often equal to or greater than the maximum speed defined by the reference profile, the optimizer is sometimes allowed to slightly exceed the baseline speed, thus expanding its room for maneuver. Moreover, slope variation plays a critical role in the optimization process. A common strategy observed is to decelerate during uphill sections and accelerate on downhill gradients, which helps reduce overall energy consumption.

This is particularly relevant given that the vehicle is equipped with regenerative braking, allowing it to recover energy during deceleration. As a result, the optimizer can afford more aggressive braking than the reference profile, without compromising efficiency. Overall, on these urban segments, the eco-driving strategy proves to be highly effective, yielding energy savings in the range of 5 to 10%, which is a significant improvement.

Conversely, other parts of the route involve constant-speed segments typical of long-distance highways. In such cases, the optimizer has fewer degrees of freedom due to the lack of speed variability across segments. Additionally, the optimization algorithm is constrained to match the segment travel time defined by the reference profile, further limiting its capacity to reduce energy consumption.

The remaining degrees of freedom are limited to slight adjustments in speed—above or below the reference maximum—and leveraging altitude variations. In these situations, the optimizer typically increases speed during downhill sections and reduces it during uphill climbs, thereby easing the load on the powertrain and minimizing energy use. Even so, the optimization margins are small, and the resulting energy savings are limited to only a few percent, as evidenced in the data.

This project has received funding from the European Union's HORIZON EUROPE research and innovation programme under grant agreement No. 101096028. The content of this publication is the sole responsibility of the Consortium partners listed herein and does not necessarily represent the view of the European Commission or its services.

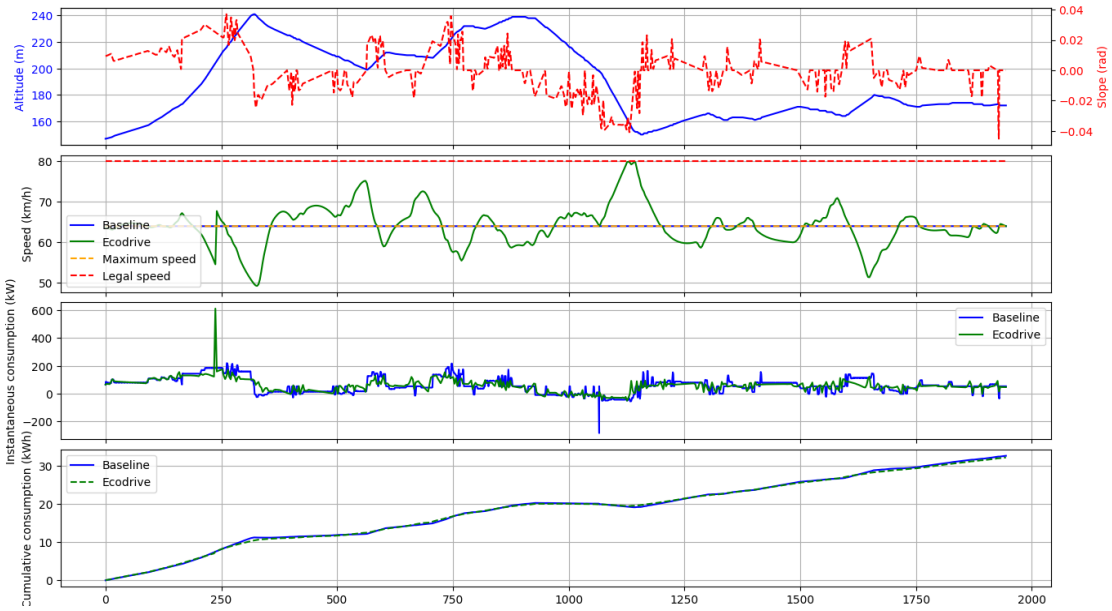

Figure 43: Analysis of constant-speed segments (altitude, speed, speed and consumptions as function of time)

When applying the eco-driving strategy to the full Ulm–Verona route, the results show a clear improvement in energy efficiency. The total energy consumption was reduced by approximately 7.05%, corresponding to an energy saving of 35.96 kWh, with a final optimized consumption of 473.99 kWh.

Out of the total 508.6 km, the eco-driving algorithm optimized around 84.65% of the route. While the route mainly consisted of high-speed, constant-velocity segments, which offer fewer opportunities for significant energy savings, the results still demonstrate the effectiveness of the strategy. It's important to note that if the route had included more urban or variable-speed sections, the potential for optimization would have been even greater, as the algorithm could have made more adjustments to speed and energy use. Despite this, the current results show promising improvements in energy consumption for long-distance journeys.

This project has received funding from the European Union's HORIZON EUROPE research and innovation programme under grant agreement No. 101096028. The content of this publication is the sole responsibility of the Consortium partners listed herein and does not necessarily represent the view of the European Commission or its services.

4 Bibliography

[1] Dhevathi Rajan Rajagopalan Kannan, "An Introduction to Fast Charging and Pulse Charging," BatteryBits (Volta Foundation). Accessed: Apr. 04, 2025. [Online]. Available: https://medium.com/batterybits/an-introduction-to-fast-charging-and-pulse-charging-21cd21a599ae.

[2] J. H. Ahn and B. K. Lee, "High-Efficiency Adaptive-Current Charging Strategy for Electric Vehicles Considering Variation of Internal Resistance of Lithium-Ion Battery," *IEEE Trans Power Electron*, vol. 34, no. 4, pp. 3041–3052, Apr. 2019, doi: 10.1109/TPEL.2018.2848550.

[3] Z. Chen, B. Xia, C. C. Mi, and R. Xiong, "Loss-Minimization-Based Charging Strategy for Lithium-Ion Battery," *IEEE Trans Ind Appl*, vol. 51, no. 5, pp. 4121–4129, Sep. 2015, doi: 10.1109/TIA.2015.2417118.

[4] Q. Dang, D. Wu, and B. Boulet, "EV Fleet as Virtual Battery Resource for Community Microgrid Energy Storage Planning," *IEEE Canadian Journal of Electrical and Computer Engineering*, vol. 44, no. 4, pp. 431–442, 2021, doi: 10.1109/ICJECE.2021.3093520.

[5] A. Golder and S. S. Williamson, "Energy Management Systems for Electric Vehicle Charging Stations: A Review," in *IECON Proceedings (Industrial Electronics Conference)*, IEEE Computer Society, 2022. doi: 10.1109/IECON49645.2022.9968614.

[6] A. S. A. Awad, M. F. Shaaban, T. H. M. El-Fouly, E. F. El-Saadany, and M. M. A. Salama, "Optimal Resource Allocation and Charging Prices for Benefit Maximization in Smart PEV-Parking Lots," *IEEE Trans Sustain Energy*, vol. 8, no. 3, pp. 906–915, Jul. 2017, doi: 10.1109/TSTE.2016.2617679.

[7] D. Wang, F. Locment, and M. Sechilariu, "Modelling, simulation, and management strategy of an electric vehicle charging station based on a DC microgrid," *Applied Sciences (Switzerland)*, vol. 10, no. 6, Mar. 2020, doi: 10.3390/app10062053.

[8] C. Xu *et al.*, "Electric vehicle batteries alone could satisfy short-term grid storage demand by as early as 2030," *Nat Commun*, vol. 14, no. 1, Dec. 2023, doi: 10.1038/s41467-022-35393-0.

[9] I. Chandra, N. K. Singh, P. Samuel, M. Bajaj, and I. Zaitsev, "Coordinated charging of EV fleets in community parking lots to maximize benefits using a three-stage energy management system," *Sci Rep*, vol. 14, no. 1, Dec. 2024, doi: 10.1038/s41598-024-83579-x.

[10] J. Shi, T. Zeng, and S. Moura, "Electric fleet charging management considering battery degradation and nonlinear charging profile," *Energy*, vol. 283, Nov. 2023, doi: 10.1016/j.energy.2023.129094.

[11] J. C. Gillett, F. Southworth, M. Meyer, and A. Amekudzi, "Monetizing truck freight and the cost of delay for major truck routes in Georgia" Dec. 2011.

[12] R. M. Aldrete, D. Salgado, S. Samant, and M. V. Ostos, "Estimating economic impact of commercial vehicle border delays in real time" Texas, Sep. 2018.

[13] F. H. A. (FHWA) U.S. Department of Transportation, "Freight Transportation Costs [Office of Freight Management and Operations]," https://ops.fhwa.dot.gov/freight/freight_analysis/freight_story/costs.htm.

[14] Alanazi, F. (2023). Electric vehicles: Benefits, challenges, and potential solutions for widespread adaptation. *Applied Sciences*, *13*(10), 6016.

[15] C. Ngo, F. de Smet, Olivier Lemaire, M. Espig, Giovanni de Nunzio, et al.. Connected strategy for energy-efficient driving of electric vehicle. SIA - Powertrain & Energy, Jun 2022, Rouen, France. ⟨hal-03890407⟩

[16] D2.4 Generic eco-driving strategy—LONGRUN project. Horizon 2020.

[17] Sciarretta, A., De Nunzio, G., & Ojeda, L. L. (2015). Optimal ecodriving control: Energy-efficient driving of road vehicles as an optimal control problem. *IEEE Control Systems Magazine*, *35*(5), 71–90.

[18] D2.1 Design of fully integrated e-axle and associated control—EMPOWER project. Horizon 2020.

[19] Sciarretta, A., Vahidi, A., & others. (n.d.). Energy-efficient driving of road vehicles. Springer.

This project has received funding from the European Union's HORIZON EUROPE research and innovation programme under grant agreement No. 101096028. The content of this publication is the sole responsibility of the Consortium partners listed herein and does not necessarily represent the view of the European Commission or its services.

[20] Schoenberg, S., & Dressler, F. (2019, October). Planning Ahead for EV: Total Travel Time Optimization for Electric Vehicles. *2019 IEEE Intelligent Transportation Systems Conference (ITSC)*.

[21] De Nunzio, G., Ben Gharbia, I., & Sciarretta, A. (2020). A Time- and Energy-Optimal Routing Strategy for Electric Vehicles with Charging Constraints. *2020 IEEE 23rd International Conference on Intelligent Transportation Systems (ITSC)*, 1–8. https://doi.org/10.1109/ITSC45102.2020.9294622

[22] Morlock, F., Mammel, C., Engelhardt, T., & Sawodny, O. (2020). Trip Planning for Electric Vehicles Considering the Available Charging Infrastructure. *2020 IEEE International Conference on Industrial Technology (ICIT)*, 723–728. https://doi.org/10.1109/icit45562.2020.9067111

[23] Qian, Q., Gan, M., Wei, L., Yao, Z., & He, Y. (2024). Behavior-Driven Planning of Electric Truck Charging Infrastructure for Intercity Operations. *IEEE Transactions on Intelligent Transportation Systems*, *25*(9), 12049–12065. https://doi.org/10.1109/tits.2024.3375458

[24] Zähringer, M., Teichert, O., Balke, G., Schneider, J., & Lienkamp, M. (2024). Optimizing the Journey: Dynamic Charging Strategies for Battery Electric Trucks in Long-Haul Transport. *Energies*, *17*(4), 973. https://doi.org/10.3390/en17040973

[25] Bragin, M. A., Ye, Z., & Yu, N. (2023). Toward Efficient Transportation Electrification of Heavy-Duty Trucks: Joint Scheduling of Truck Routing and Charging. *Transportation Research Part C: Emerging Technologies*. https://doi.org/10.48550/ARXIV.2302.00240

[26] Zhu, J., Michel, P., Zonetti, D., and Sciarretta, A., "A Bi-Level Optimization Approach for Eco-Driving of Heavy-Duty Vehicles," SAE Technical Paper 2023-24-0172, 2023, https://doi.org/10.4271/2023-24-0172.

This project has received funding from the European Union's HORIZON EUROPE research and innovation programme under grant agreement No. 101096028. The content of this publication is the sole responsibility of the Consortium partners listed herein and does not necessarily represent the view of the European Commission or its services.

5 Acknowledgment

European Union's HORIZON EUROPE research and innovation programme

This project has received funding from the European Union's HORIZON EUROPE research and innovation programme under grant agreement No. 101096028. The content of this publication is the sole responsibility of the Consortium partners listed herein and does not necessarily represent the view of the European Commission or its services.

Project Partners:

The author(s) would like to thank the partners in the project for their valuable comments on previous drafts and for performing the review.

Participant No*	Participant short name	Participant organisation name	Country
1 Coordinator	**AIT**	AIT Austrian Institute of Technology GmbH	AT
2	**IVECO**	IVECO SPA	IT
3	**FPT**	FPT Industrial SPA	IT
4	**IFPEN**	IFP Énergies nouvelles	FR
5	**POLITO**	Politecnico di Torino	IT
6	**LT**	Lead Tech SRL	IT
7	**VIL**	Villinger GmbH	AT
8	**CID**	Fundación CIDETEC	ES
9	**CTE**	CT Engineering GmbH	AT
10	**GLO**	GRUBER Logistics S.p.A.	IT
11	**BRE**	BREMBO SPA	IT
12	**IIT**	Istituto per Innovazioni Tecnologiche Bolzano S.c.a.r.l.	IT
13	**ALFI**	Air Liquide	FR
14	**FMF**	FPT Motorenforschung AG	CH